Effects of wave forcing on a subterranean estuary

Pei Xin[1,2#], Clare Robinson[3], Ling Li[2,1], D. A. Barry[4], R. Bakhtyar[4]

[1]Centre for Eco-Environmental Modelling, Hohai University, Nanjing, P. R. China

Email: p.xin@uq.edu.au

[2]National Centre for Groundwater Research and Training, School of Civil Engineering, The University of Queensland, Queensland, Australia

Emails: p.xin@uq.edu.au

l.li@uq.edu.au

[3]Department of Civil and Environmental Engineering, The University of Western Ontario, London, N6A5B9, Canada

Email: crobinson@eng.uwo.ca

[4]Laboratoire de technologie écologique, Institut d'ingénierie de l'environnement', Ecole Polytechnique Fédérale de Lausanne (EPFL), Station 2, CH-1015, Lausanne, Switzerland

Emails: andrew.barry@epfl.ch

roham.bakhtyar@epfl.ch

Re-submitted to *Water Resources Research* on 23 September 2010

[#] Author to whom all correspondence should be sent. Email: p.xin@uq.edu.au

Abstract

Wave and tide are important forcing factors that typically co-exist in coastal environments. A numerical study was conducted to investigate individual and combined effects of these forces on flow and mixing processes in a near-shore subterranean estuary. A hydrodynamic model based on the shallow water equations was used to simulate dynamic sea level oscillations driven by wave and tide. The oscillating sea levels determined the seaward boundary condition of the coastal aquifer, where variably-saturated, variable-density flow was modeled. The simulation results showed that waves induced an onshore upward tilt in the phase-averaged sea level (wave set-up). The resulting hydraulic gradient generated pore water circulations in the near-shore zone of the coastal aquifer, which led to formation of an upper saline plume (USP) similar to that formed due to tides. However, mixing of recirculating seawater in the USP with underlying fresh groundwater was less intensive under the high-frequency wave oscillations. In the case of combined forcing, wave-induced circulations coupled with the intra-tidal flows strengthened the averaged, circulating pore water flows in the near-shore zone over the tidal period. The circulating flows increased exchange between the subterranean estuary and ocean, contributing 61% of the total submarine groundwater discharge for the simulated condition in comparison with the 40% and 49% proportions caused by the same but separate tidal and wave forcing, respectively. The combined forces also created a more extensive USP with the freshwater discharge zone shifted further seaward. The freshwater flow paths in the intertidal subterranean estuary were modified with a significant increase in the associated transit times. The interplay of wave and tide led to increased mixing between discharging fresh groundwater and recirculating seawater. These results further demonstrate the complexity of near-shore groundwater systems and have implications for future investigations on the fate of land-sourced chemicals in the subterranean estuary prior to discharge to the ocean.

Keywords: ocean-land interaction; submarine groundwater discharge; near-shore processes; pore water flow; solute transport; coastal water quality

1. Introduction

Currently more than 40% of the world population lives within 100 km from the coastline [*Martínez et al.*, 2007]. The rapid development of coastal areas has increased the amount of pollutants discharged into coastal seas. Traditionally surface water, flowing through rivers and estuaries to the sea, has been considered to be the main and often sole carrier of these pollutants [*Moore*, 1999]. However, it is now widely recognized that submarine groundwater discharge (SGD) also provides a significant transport pathway for chemicals entering the marine environment [*Moore*, 1996; *Li et al*., 1999; *Robinson et al*., 2007a; *Moore*, 2010]. Generally, the groundwater discharge at the shoreline comprises terrestrially derived freshwater (Q_f) and recirculated seawater (SGR) [*Taniguchi et al*., 2002], i.e.,

$$\mathrm{SGD} = Q_f + \mathrm{SGR} \tag{1}$$

The SGR is composed of three major components due to density-driven flow (Q_d), tidally-driven flow (Q_t) and wave-induced flow (Q_w) as shown in Fig. 1, i.e.,

$$\mathrm{SGR} = Q_d + Q_t + Q_w \tag{2}$$

On the subsurface pathway from the land source to the sea, pollutants are transported through a mixing zone similar to a surface estuary, hence called subterranean estuary [*Moore*, 1999]. The fates of pollutants in a subterranean estuary are determined by local flow, transport and reaction processes.

Flows in a subterranean estuary are influenced by the forcing provided by the inland hydraulic gradient. In the absence of oceanic forces, fresh groundwater (carrying land-sourced chemicals) flows on top of a saltwater wedge (SW) prior to discharge to the ocean around the shoreline. A transition zone exists between the seawater in the saltwater wedge and the overlying freshwater, where the concentration of salt varies from the concentration of seawater to that of inland freshwater (Fig. 1). Across the transition zone, hydrodynamic dispersion causes salt to disperse into the freshwater zone, which in turn drives the convective circulation through the wedge [*Cooper*, 1959]. This transition/dispersion zone was traditionally considered as the primary area of mixing between discharging fresh groundwater and recycling seawater in the subterranean estuary [*Moore*, 1999].

At most natural coasts, the subterranean estuary is also exposed to the influence of oceanic oscillations, including tides and waves. Tidal effects have been examined extensively in many recent studies based on numerical modeling [*Prieto and Destouni*, 2005; *Mao et al*., 2006; *Brovelli et al.*, 2007; *Robinson et al*., 2007a,b; *Robinson et al*., 2009; *Li et al*., 2008; *Maji and Smith*, 2009; *Li et al.*, 2009], field measurements [*Vandenbohede and Lebbe*, 2005; *Robinson et al*., 2006] and laboratory experiments [*Boufadel*, 2000; *Robinson and Li*, 2004; *Colbert et al.*, 2008; *Anschutz et al.*, 2009]. It has been revealed that tidal sea level oscillations induce relatively rapid recirculation of large amounts of seawater through the subterranean estuary, which contributes significantly to the SGD. Salt transport associated with the seawater recirculation leads to the formation of an upper saline plume in the intertidal region (USP in Fig. 1). Compared with the lower saltwater wedge, the USP acts as a potentially more important mixing and reaction zone, and thus may influence significantly the fate of pollutants in the subterranean estuary. Under the tidal influence, the freshwater flows around the USP, lengthening the flow paths and in turn increasing the transit times along the paths [*Robinson et al*., 2007a].

Waves in the near-shore zone are another important oceanic forcing factor for the subterranean estuary. While waves induce instantaneous pore water flows in response to individual bores and wave run-up, these flows are rapidly attenuated in the beach sediment due to the high frequency [*Li and Barry*, 2000; *Horn*, 2006]. However, the phase-averaged effects of waves may strongly influence the near-shore groundwater behavior. As the wave breaks, the resulting energy dissipation and changes in the onshore radiation stress induce an onshore upward tilt in the mean sea level (MSL) (i.e., wave set-up as shown in Fig. 1; [*Sorenson*, 2006]). This creates hydraulic gradients on the beach surface, which drive circulations with seawater infiltrating the upper part of the beach and exiting the beach groundwater system near the wave-breaking point, as predicted analytically by

Longuet-Higgins [1983]. Through numerical simulations, *Li and Barry* [2000] found that wave run-up also contributes to the seawater circulation. Their study further showed that the circulation was affected by the beach groundwater table elevation relative to the MSL. However, both studies ignored density variations of pore water and associated density-dependent flows in the subterranean estuary.

Moore's [1996] field study showed that, in a large coastal area, SGD could amount to as much as 40% of the total river flow into the ocean. His estimate was inferred from a mass balance based on measurements of enriched radium-226 in the South Atlantic Bight. *Younger* [1996] argued that the recharge to the coastal aquifer was not sufficient to sustain such a high rate of SGD. The aquifer recharge alone could support only 4% of the estimated SGD. Subsequently, *Li et al.* [1999] presented a theoretical model of flow and chemical transport processes in subterranean estuaries. This model predicted that seawater circulation, caused by wave set-up and tide, may constitute up to 96% of the total SGD. Recently *Robinson et al*. [2007a] simulated in detail the flow processes in a hypothetical, tidally influenced subterranean estuary and found that tide-induced and density-driven seawater circulations contributed, respectively, 45.5% and 19% of the total SGD. As discussed above, wave action is also likely to influence the subterranean estuary. Previous investigations of wave effects on the near-shore groundwater have focused on the behavior of groundwater table fluctuations [*Turner et al.*, 1997; *Nielsen*, 1999; *Cartwright et al.*, 2004]. A numerical study on the beach groundwater flow affected by high-frequency waves was recently carried out by *Bakhtyar et al*. [2010]. However, to our knowledge, the response of a subterranean estuary to waves has not been examined in terms of flow and transport characteristics. In particular, little is known about the role played by waves in controlling the mixing and exchange between freshwater and recirculated seawater in the subterranean estuary. Therefore, how waves affect the subterranean estuary remains an unresolved question. Moreover, as waves and tides co-exist at most natural coasts, understanding the interplay of both forces is essential for quantifying flow and solute transport processes in the subterranean estuary.

This numerical study aimed to examine and quantify the individual and combined effects of waves and tides on the pore water flow and salt transport in the near-shore zone of a subterranean estuary. BeachWin [*Li et al.*, 2002], a near-shore wave model based on the shallow water flow equations, was used to simulate sea level oscillations driven by wave and tide. The simulated, oscillating sea levels were then used to define the seaward boundary condition of a variably-saturated, variable-density flow model of the coastal aquifer, based on SUTRA [*Voss and Provost*, 2002]. Simulations were conducted under various forcing conditions: without oceanic forcing, with only tidal forcing, with only wave forcing, and with combined wave and tidal forcing. The simulation results were analyzed to generate insight into the complex behavior of the subterranean estuary under the influence of waves separately and also in combination with tides.

2. Mathematical models and simulations

2.1. Governing equations and boundary conditions

The model focused on the cross-shore section of a coastal aquifer, assuming negligible flow and solute transport in the alongshore direction (Fig. 1). The two-dimensional variably-saturated, variable-density flow is described by:

$$\partial(\rho\phi S_W)/\partial t = -\nabla\cdot\left(\rho\vec{q}\right) + \rho_s Q \tag{3a}$$

with

$$\vec{q} = -K(\psi)\nabla\left(\frac{P}{\rho g} + z\right) \tag{3b}$$

where $\vec{q}$ is the Darcy flux [LT^{-1}]; t is the time [T]; $K(\psi)$ is the hydraulic conductivity [LT^{-1}]; ψ is the capillary pressure head [L]; S_W is the soil saturation [-]; ϕ is the soil porosity [-]; g is the magnitude of the gravitational acceleration [LT^{-2}]; P is the pore water pressure [ML^{-1}T^{-2}]; Q is the fluid source [L^{3}T^{-1}]; z is the elevation [L]; ρ_s is the density of fluid source [ML^{-3}] and ρ is the fluid density [ML^{-3}] that varies with the salt concentration according to $\rho = \rho_0 + \frac{\partial\rho}{\partial C}C$, where

ρ_0 is the freshwater density [ML^{-3}], C is the salt concentration (mass fraction) [-], and $\frac{\partial \rho}{\partial C}$ is used to describe the linear relationship between fluid density and salt concentration, and is given by: $\frac{\partial \rho}{\partial C} = 714.3$ kg m^{-3}.

Note that the sediment storativity due to the compressibility of fluid and sediment matrix is neglected in equation (3a). The standard method for quantifying the compressibility-induced sediment storativity is based on the assumption of constant total stress on the porous medium and hence $\Delta\sigma_e$ (change of effective stress) = $-\Delta P$ (change of pore water pressure) since σ_T (total stress) = σ_e (effective stress) $+ P$ (pore water pressure). On the beach surface, fluctuations of pore water pressure with varying depths of overlying water would lead to changes of effective stress under the assumption of constant total stress, generating an artificial pressure wave through the elastic sediment. However, the total stress on the beach sediment is not constant and varies in the same way as the pore water pressure, thus giving an invariant effective stress (i.e., no expansion or contraction of sediment matrix). To account for the total stress variation and remove the artificial pressure wave, a tidal loading term needs to be incorporated into Richards' equation [*Reeves et al.*, 2000; *Gardner and Wilson*, 2006; *Maji and Smith*, 2009]. On the other hand, numerical tests [*Xin et al.*, 2009] showed that if the saturated hydraulic conductivity of sediments is larger than 10^{-6} m/s, the compressibility plays a negligible role in governing the groundwater flow in the sediment. Under such a condition, an alternative, simpler approach for dealing with the total stress variation is to neglect the compressibility terms in the governing equation, in which case the tidal loading modification for Richards' equation is no longer required [*Xin et al.*, 2009]. Given that the beach simulated here satisfies this condition, we adopted the second approach with the compressibility of fluid and sediment matrix neglected.

Coupled with the pore water flow, the salt solute transport in the porous medium is governed by the transport equation:

$$\partial(\rho\phi S_W C)/\partial t = -\nabla\cdot\ \rho\vec{q}C\ +\nabla\cdot\ \rho\phi S_W\mathbf{D}\nabla C\ +\rho_s Q C^* \tag{4}$$

where $\mathbf{D}$ is the hydrodynamic dispersion tensor [L^2T^{-1}]; and C^* is the salt concentration of the fluid source [-]. The relative hydraulic conductivity and the soil saturation were calculated using the *van Genuchten* [1980] formulas:

$$S_W = S_{Wres} + \ 1 - S_{Wres}\ \left[\frac{1}{1+(\alpha\psi)^n}\right]^{\left(\frac{n-1}{n}\right)} \tag{5}$$

$$K(\psi) = K_S S_W^{*\,1/2}\left\{1-\left[1-S_W^{*\left(\frac{n}{n-1}\right)}\right]^{\left(\frac{n-1}{n}\right)}\right\}^2 \quad \text{with} \quad S_W^* = \frac{S_W - S_{Wres}}{1-S_{Wres}} \tag{6}$$

where K_S is the saturated hydraulic conductivity [LT^{-1}]; S_{Wres} is the residual water saturation [-]; and α [L^{-1}] and n [-] are constants.

In the present paper, the *x-z* co-ordinate origin was set at the mean shoreline. Coordinates of reference points of the model domain are given in Table 1. The aquifer thickness was 30 m at the mean shoreline, decreased offshore due to the sea bed slope and increased landward with the rising mean groundwater table. No areal recharge to or evapotranspiration from the aquifer was considered and hence no water or solute flux occurred across the boundary **AF** (Fig. 1). The aquifer base, **BC,** was assumed to be impermeable (zero flux). The inland boundary **AB**, was set far from the shore (much further landward than the subterranean estuary) and located at x = -150 m. This boundary was specified with a freshwater discharge (Q_f) of 2.1 m^3/d per unit width and a background salt concentration of 1 ppt (parts per thousand, i.e., grams of salt per kilogram of solution). To enable comparison between studies, the Q_f adopted was the same as that used in the previous modeling study of *Robinson et al.* [2007a]. The seaward boundary **DC** was also set sufficiently far from the shoreline so that it would not affect the simulation results for the near-shore subterranean estuary. In the simulations presented here, **DC** was located at x = 50 m and specified as no flux boundary (water and solute). The boundary condition on the aquifer-ocean interface (**DEF)** depended on the sea surface elevation, which fluctuated with wave and tide. Below the sea surface, the (submerged) boundary nodes were prescribed by hydrostatic pressure according to the local water depth given by the sea level. Above the sea surface, two cases were considered: (1) if the (exposed) nodes were saturated at the previous time step, they were taken as seepage face nodes with local pressure equal to the atmospheric pressure (i.e., P = 0); and (2) if the nodes were unsaturated, they were treated as part of a no flow boundary (more details can be found in *Xin et al.*, [2009]).For salt transport, the seawater concentration (35 ppt) applied where inflow (to the aquifer) occurred and zero concentration gradient was specified at nodes with outflow (from the aquifer).

2.2. Simulation of sea surface oscillations using BeachWin

To determine the boundary condition on the aquifer-ocean interface (**DEF)** as discussed above, BeachWin [*Li et al.*, 2002] was used to simulate the sea surface oscillations driven by wave and tide. This model is based on the depth-averaged shallow water equations [*Hibberd and Peregrine*, 1979]:

$$\frac{\partial h}{\partial t}+\frac{\partial}{\partial x}(hu)=0 \tag{7a}$$

$$\frac{\partial}{\partial t}(hu)+\frac{\partial}{\partial x}(hu^2+\frac{1}{2}gh^2)=-\tan(\gamma)gh \tag{7b}$$

where h and u are the depth [L] and depth-averaged flow velocity [LT^{-1}] of the seawater, respectively; γ is the beach angle [-]; and x is the horizontal coordinate with the origin defined at the intersection of the beach surface with the averaged mean sea level [L].

A prescribed incoming wave was combined with the tide and reflective wave (calculated from the numerical solution based on the linear wave theory) to determine the seaward boundary conditions for the wave model [*Kobayashi et al*., 1987], i.e.,

$$H(t)=Z_{MSL}+A_t\sin(\omega_t t)+A_w\sin(\omega_w t) \tag{8}$$

where $H(t)$ is the deep water sea level, oscillating with wave and tide [L]; Z_{MSL} is the averaged mean sea level [L]; A_t and A_w [L] are the amplitudes of the tide and wave, respectively; ω_t and ω_w [T^{-1}] are the angular frequencies of the tide and wave, respectively ($\omega=2\pi/T$ with T being the period [T]). The landward boundary was the moving shoreline. An extrapolation-correction-smoothing procedure developed by *Hibberd and Peregrine* [1979] was applied to determine the moving shoreline for every time step. With these boundary conditions, equations (7) were solved to predict the oscillating sea surface elevations in the near-shore zone.

2.3. Parameter values used in the simulations and approaches of coupling wave and tide

The model setup was largely similar to that used by *Robinson et al*. [2007a] except for the wave forcing condition and unsaturated flow. The aquifer with a sloping beach (slope = 0.1) was assumed to be isotropic and homogeneous with K_S = 10 m/d, ϕ = 0.45, longitudinal dispersivity α_{L} = 0.5 m and transverse dispersivity α_{T} = 0.05 m. S_{Wres} was set to 0.1 while the *van Genuchten* [1980] water retention parameters n and α were set to 14.5 m^{-1} and 2.68, respectively. These parameter values are representative of sands [*Carsel and Parrish*, 1988] commonly encountered in near-shore aquifers.

Four cases with different oceanic forcing conditions were simulated, where the coastal boundaries were respectively subjected to the influence of:

Case 1, a static (constant) sea level;

Case 2, a semi-diurnal (T_t = 12 h) tide with amplitude A_t = 1 m;

Case 3, a typical swell wave with a period T_w = 10 s and amplitude A_w = 0.2 m; and

Case 4, combined wave (T_w = 10 s; A_w = 0.2 m) and tide (T_t = 12 h; A_t = 1 m).

The combined effects of wave and tide on the sea level were simulated explicitly by the wave model (BeachWin), which provided predictions of sea level oscillations at very small time steps (~0.01 s) within each wave cycle over the tidal period. To apply directly such high-frequency oscillations to drive the simulation of the variably-saturated, variable-density groundwater flow in the near-shore zone would require use of small time steps in the SUTRA-based subterranean estuary model. On the other hand, the simulation needs to run for a very long time to resolve the tidal oscillations. This resulted in an extremely high computational cost, which prohibited the direct (phase-resolving) simulation. Therefore, a phase-averaged approach was explored. With this approach, the simulated dynamic sea levels were averaged over the wave period to generate phase-averaged sea levels. These averaged sea levels, which contained the wave set-up effect and fluctuated with the tide, were then set as the boundary condition on the aquifer-ocean interface to drive the flow model of the subterranean estuary. We conducted the Case 3 simulation using both phase-resolving (i.e., considering the dynamic wave process) and phase-averaged sea levels to define the seaward boundary condition. Similar results were obtained, suggesting that the main wave effect on the subterranean estuary is due to wave set-up and thus the phase-averaged approach, retaining this key effect, provides an effective and efficient way of representing the wave forcing, especially in combination with the tide (detailed discussion in Section 3.1).

The model was run with a time step of 10 s (one wave cycle) for all simulations except Case 3 with the phase-resolving approach, which used a relatively small time step (~0.1 s, 10 times the time step used in the BeachWin-based wave simulation). The same mesh generated with 31,191 nodes and 30,080 elements was used in all cases. Typically, the local mesh around the aquifer-ocean interface (where the USP was expected to form) was refined with $\Delta x = 0.33$ m and $\Delta z = 0.1$ m. As suggested by *Voss and Provost* [2002], the stability criterion based on the Péclet number ($P_e \leq 4$) was enforced in the simulations to avoid numerical oscillations. A series of numerical tests with time steps and mesh sizes reduced sequentially were conducted to ensure that the simulation results were independent of time step and mesh size, and thus can be considered as converged numerical solutions to the mathematical model.

Following the approach by *Robinson et al*. [2007a], the model was initially run to the steady state with a static sea level (Z_{MSL}). Oceanic forcing was then introduced according to the case simulated. The model was run for a sufficiently long time to reach the quasi-steady state (i.e., the periodic solution) with respect to both heads and concentrations. The test on the quasi-steady state was based on changes in heads (similarly for concentrations) over a given cycle (tidal period) evaluated at a set of representative points within the domain being less than 10^{-4} m. For example, for Case 2 with the tide, heads reached the quasi-steady state approximately 200 d after the simulation started, but the quasi-steady state for concentrations took approximately 600 d.

3. Simulation results and discussions

3.1. Wave effects: Circulating flows, and salt transport and distribution

Wave transformation in the near-shore zone is a non-linear process, which leads to wave steepening and breaking. As a result of wave breaking and subsequent wave energy dissipation, the averaged sea level over the wave period tilts upward in the onshore direction (i.e., the wave set-up). *Longuet-Higgins* [1983] demonstrated analytically that wave set-up induces pore water circulation underneath the beach. *Li and Barry* [2000] and *Bakhtyar et al*. [2010] simulated numerically dynamic responses of beach groundwater to wave and found similar circulation patterns in the averaged groundwater flow field. Here, we examined further the wave effects on the near-shore groundwater flow behavior, taking into account variable densities due to salt transport. Both the phase-resolving and phase-averaged approaches were adopted to distinguish the relative importance of the time-averaged wave effects and instantaneous wave-induced flow oscillations.

The instantaneous pore water flows in the near-shore zone, simulated with the phase-resolving approach, are shown in Fig. 2. The dynamic nature of the flow was clearly evident. Driven by hydraulic gradients associated with the fluctuating sea surface, the pore water flow oscillated. The overall flow was also characterized by spatial patterns with persistent inflow and outflow near the maximum wave run-up and wave-breaking point, respectively. Large hydraulic gradients associated with steep wave fronts generated shallow circulation cells that moved across the beach as the wave ran up and down (Figs. 2c-2f). These moving, localized circulations, observed previously by *Li and Barry* [2000], did not cause significant net flux since the influx and efflux across the aquifer-ocean interface largely canceled out. The phase-averaged flow field and sea surface elevation, calculated from the instantaneous results, exhibited a distinctive circulation cell and onshore tilt of the sea surface, which were evidently linked (Fig. 3a).

The phase-averaged approach neglected the dynamic sea level oscillations and instead used the averaged sea surface elevation to specify the seaward boundary condition of the subterranean estuary model. However, the predicted flow, also characterized by a circulation pattern, closely resembled the averaged flow from the phase-resolving simulation (Fig. 3a). The total circulation rate based on the phase-averaged approach was calculated to be 2.23 m^3/d per unit width, reasonably close to that predicted using the phase-resolving approach, 2.53 m^3/d per unit width (Table 2). Moreover, salt transport associated with the circulating flow (i.e., seawater recirculation) formed similar salt distributions in the near-shore zone for both modeling approaches. In particular, the upper saline plumes generated by the circulation in both cases appeared to have the same extent, including similar saltwater-freshwater mixing zones. The similarity was demonstrated in the comparison of the contours of the predicted salt concentrations from the phase-resolving and phase-averaged simulations (Fig. 3b). The wave-induced flow oscillations as predicted by the phase-resolving simulation slightly increased the landward extent of the circulation cell and widened a little the mixing zone near the discharge area (wave-breaking point). Except for these relatively small differences in the near-surface areas, the concentration contours predicted by both approaches virtually overlapped, suggesting that instantaneous wave-induced flow oscillations did not affect significantly the circulating flow and associated salt transport. Therefore, the dominant wave effect was well captured by the wave set-up of the averaged sea surface (note that the wave run-up effect was also included in determining the tilt of the averaged sea surface).

To further examine the wave effects on the subterranean estuary, we compared the simulation results discussed above with those from Cases 1 and 2 (Fig. 4). In the absence of oceanic forcing (Case 1), the classical salt distribution was simulated with fresh groundwater overlying the saltwater wedge. Mixing between fresh groundwater and seawater occurred in the dispersion zone of the wedge. With the forcing imposed by tide (Case 2) and wave (Case 3), the salt distribution in the subterranean estuary changed significantly with the formation of the USP near the beach surface (Figs. 5 and 6). The tidal simulation results were similar to those of *Robinson et al*. [2007a], who modeled the same condition. The USPs in both cases were associated with seawater recirculation driven by phase-averaged hydraulic gradients at the beach surface (i.e., the aquifer-ocean interface). In the wave case, the averaged hydraulic gradients were linked to the onshore upward tilt of the averaged sea surface, which led to increases in hydraulic heads at the boundary from the wave-breaking point to the maximum wave run-up (Fig. 7). The rate of the spatial head increase, given by the onshore slope of the averaged sea surface, was estimated to be around 0.032. Due to seepage face and non-linear effects of tidal forcing on the sloping beach, similar hydraulic gradients were also generated by the tide acting on the sloping beach. Averaged hydraulic heads at the beach surface, calculated based on the tidal simulation results, exhibited an onshore increase at a rate of 0.033 within the intertidal zone (Fig. 7). Although the rates of the spatial head increase, representing the magnitude of the hydraulic gradients at the boundary, were similar in both cases, the extent of the intertidal zone was greater than that of the combined surf and swash zone, resulting in a more extensive USP in the tidal case. Nevertheless, the mechanism of the circulation and USP formation was the same in the tidal and wave cases, both driven by the averaged head gradient at the aquifer-ocean interface. It is interesting to note that the formation of the USP pushed the lower saltwater wedge offshore. This phenomenon was also observed by *Robinson et al*. [2007a]. The extent of the offshore shift of the wedge corresponded with the size and location of the USP.

Despite the similarity, the wave- and tide-induced USPs differed significantly in the thicknesses of their mixing zones. While the wave did not seem to induce significant mixing of the recirculating seawater in the USP with underlying fresh groundwater, the tidal oscillations intensified the mixing and led to thickening of the USP's mixing zone (and that of the saltwater wedge). In both cases, the oceanic forcing induced pore water flow oscillations in the near-shore area. Such flow oscillations may enhance the mixing with an increased (apparent) dispersion coefficient. Based on the turbulence dispersion concept [*Fischer et al.*, 1979], we suggest that the increased mixing intensity or apparent dispersion coefficient (D_a) is related to,

$$D_a \propto \sigma_u t_c \tag{9}$$

where σ_u and t_c are the variance and characteristic time scale of the flow oscillations, respectively, with t_c determined by the period of the oscillations. As an example, we show the oscillating flow velocities at a central location of the USP's mixing zone for both the wave and tidal cases (Fig. 8). Flow oscillations in both cases were of similar magnitudes. Based on the results, the variance of the flow oscillations was calculated to be 0.012 m^2/d^2 in the horizontal direction and 0.014 m^2/d^2 in the vertical direction for the wave case, and 0.250 m^2/d^2 (horizontal) and 0.018 m^2/d^2 (vertical) for the tidal case. Given that the wave period (10 s) is much smaller than the tidal period (12 h), the mixing induced by wave oscillations would be expected to be much weaker than that caused by tidal oscillations, resulting in a much narrower mixing zone.

In summary, the wave effect on the subterranean estuary is mainly manifested as circulations and associated USP driven by hydraulic gradients due to wave set-up (phase-average effect). The flow oscillations induced by the high frequency wave does not significantly enhance mixing between the recirculating seawater in the USP and freshwater underneath. It should be noted that, in the simulations, the incoming wave has been assumed to be monochromatic and of the same wave height. In reality, random waves of temporally variable height and period would induce longer period flow oscillations, which may intensify the salt and fresh water mixing.

3.2. Combined effects of wave and tide: Circulating flows, and salt transport and distribution

As demonstrated above, the phase-averaged approach provided an effective representation of the key wave effect on the subterranean estuary. This approach enabled the simulation of Case 4 with combined wave and tide forcing, which would be difficult using the phase-resolving approach due to the enormous computational demand. Based on the phase-averaged approach, sea surface elevations averaged over the wave period were calculated from the oscillating sea surface predictions by the BeachWin-based wave model. Averaged sea surface elevations, containing the wave set-up effect and fluctuating with the tide, were then used to drive the coastal groundwater model.

The results show that while the wave-induced circulation persisted during most of the tidal period, it interacted and merged with the intra-tidal flows (Fig. 9). The combined forcing strengthened the pore flows in the beach. This led to a circulation zone with an increased extent and higher flow rates compared with the results from the cases with separated tide and wave forcing. This is evident by comparing the averaged flow field over the tidal period and the salt distribution (Fig. 10). The USP extended further landward by 5.8 m and seaward by 7.3 m compared with the tidally generated USP. The horizontal expansion of the USP was accompanied by a vertical deepening by 6.3 m. Such expansion was linked to the changes in the forcing condition on the boundary. We computed the averaged hydraulic head at the beach surface. Again the results display the head variations (gradients) that drove the circulation (Fig. 7). Moreover, with wave and tide combined, the forcing zone (with onshore gradients) expanded both landward and seaward, corresponding with the expansion of the USP. The landward expansion was due to the wave action (set-up and run-up) above the high tide mark at the high tide whereas the seaward shift was due to wave breaking offshore of the low tide mark at the low tide. With the USP expansion, the lower saltwater wedge retreated further seaward (Fig. 10).

The thickness of the USP mixing zone did not change significantly compared to the case with only tidal forcing, suggesting that the mixing intensity was largely controlled by the tide-induced flow oscillations. With the expansion of the USP, the mixing zone area increased; therefore mixing of the recirculating seawater in the USP and underlying fresh groundwater was enhanced by the combined forcing. However, the opposite effect occurred in the mixing zone of the saltwater wedge with a reduced thickness, compared with the tidal case. This may be due to the influence of the ambient fresh groundwater flow. Obstructed by the USP, the freshwater flow path changed significantly with reduced flow areas and increasing flow speeds as it approached the beach surface. This steepened the interface of the saltwater wedge, which might have contributed to the thinning of the mixing zone. Also as a consequence, the potential salt transport capacity of the groundwater adjacent to the mixing zone increased. As the salt supply by the density-driven convection was limited, the increased salt transport capacity could also lead to the reduction of the mixing zone thickness.

3.3. Effects on transport path and time

The individual and combined effects of wave and tide on particle travel paths and times in the subterranean estuary were also examined. Following the method used by *Robinson et al*. [2007a], the phase-averaged flow field was used to determine the particle travel path and calculate the time it takes for a particle to travel from a certain location to the boundary of the system. For Cases 2 and 3, the particle travel path and time were also calculated using the instantaneous flow field and these were compared with the results given by the phase-averaged flow field. Both the travel path and time provide valuable information about the likelihood and extent of the particle's contact with other "particles", including different chemicals on the solid surface, and in the fresh groundwater and recirculating seawater. Such information is crucial for understanding the fate and distribution of chemicals in the system [*Zimmerman*, 1976].

Following *Robinson et al*. [2007a], particles were placed at x = -55.3 m over the depth to track the particle behavior in the freshwater zone. This initial location was treated as the landward boundary of the subterranean estuary where the tidal signal is damped to 2% of the tidal sea level oscillations [*Robinson et al*., 2007a]. Particles were also placed on the beach surface in the inflow areas to examine the particle travel path and time in the USP and lower saltwater wedge. These results are shown in Figs. 4-6 and 10.

In the freshwater zone, particle travel paths were modified significantly due to the USP formation by oceanic forcing. The travel paths, particularly for the shallow groundwater, were pushed downwards by the USP and the freshwater discharged further offshore compared with the static case

(Case 1). Both effects led to lengthening of particle travel paths and increased travel times. The extent of the path and time lengthening depended on the size of the USP, with the maximum occurred in the case of combined wave and tide forcing where the size of the USP was also the largest. Particles travelling through the USP had much shorter transit times than those in the freshwater zone (by an order of magnitude). The transit time varied slightly for the different oceanic forcing but for all cases with oceanic forcing, seawater recalculating through the USP was characterized by a short transit time. The relatively rapid recirculation of seawater through the USP provides an important mechanism for transporting chemicals of marine origin to the subterranean estuary. Coupled with mixing across the dispersion zone, this transport mechanism may strongly control the fate of land-derived chemicals in the estuary prior to discharge to the ocean. In contrast, the times for particles to move through the saltwater wedge were significantly greater (2-3 orders of magnitude difference compared with the transit times in the USP). Such long transit times imply much less influence on the chemicals in the subterranean estuary by recirculating seawater through the lower saline wedge.

To examine the effect of flow oscillations on the particle travel path and time, we also computed both quantities based on the instantaneous flow field for Cases 2 and 3. The particle was initially placed at x = 0 m and z = -7 m for Case 2 and x = -1 m and z = -5 m for Case 3, both inside the mixing zone of the USP. The results show that while the instantaneous trajectory of the particle meandered around the mean travel path (based on the phase-averaged flow field), the two pathways largely overlapped and gave similar travel times (Fig. 11). This indicates that the averaged flow field can be used to investigate the transport pathway and time of chemicals in the subterranean estuary subjected to tidal and wave forcing. The oscillatory displacement of the particle from the mean travel path however may lead to mixing in areas where solute concentration gradients exist [*Smith et al*., 2005]. As discussed in Section 3.1, a statistical parameter for characterizing such displacement and mixing is $\sigma_u t_c$. This parameter suggests that for a given similar magnitude of flow oscillations, longer period oscillations are likely to induce more significant mixing. The high frequency (small period) flow oscillations induced by waves caused much smaller displacement of the particle from its mean travel path (Fig. 11b) compared with the tidal oscillations (Fig. 11a), and therefore did not increase much the salt-freshwater mixing in the dispersion zones of the USP and saltwater wedge (Fig. 6).

3.4. Effects on groundwater fluxes and recirculation rates

To further examine the effects of wave and tide on the subterranean estuary, the water and salt fluxes across the aquifer-ocean interface were calculated. Daily local influx and efflux across the interface were calculated by integrating the simulated fluxes over the oscillation period: wave period for Case 3 using the phase-averaged approach and tidal period for Cases 2 and 4. Based on the integrated local fluxes (Figs. 12 and 13), the beach surface can be divided to three different zones: (1) freshwater discharge zone (FD) where only water outflow occurred (i.e., water influx = 0) with little salt flux; (2) upper circulation zone (UDC) landward of the FD, driven by wave (WDC), tide (TDC) or both (WTDC); and (3) lower density-driven circulation zone (DDC) offshore of the FD. The division of the zones is essentially consistent with the salt distribution near the beach surface except for the small border areas between FD and UDC, and FD and DDC, where mixing of discharging freshwater and recirculating seawater occurred (Figs. 12 and 13).

The flux pattern in Case 1 was relatively simple with a dominant efflux in the discharge zone accompanied by small amount of influx in the off-shore area due to the density-driven circulation. The efflux was largely composed of fresh groundwater with a small amount of seawater provided by the circulation (Fig. 12a). Under oceanic forcing, both the influx and efflux patterns changed dramatically. In all cases (2, 3 and 4), significant influxes occurred in the upper region of the UDC. These influxes were balanced by effluxes on the lower region of the UDC as evident in the net-fluxes, an expected result since both fluxes were parts of the same circulation system. The spatial extent of the UDC zone varied with the forcing as discussed previously and corresponded with the spatial extent of the USP along the aquifer-ocean interface. In contrast with the UDC, the lower circulation zone experienced comparatively small fluxes for all cases.

To examine further the effects of oceanic forcing on the exchange between the subterranean estuary and ocean, we calculated the total effluxes from the UDC, FD and DDC, which combined to give the total SGD. The results listed in Table 2 show that oceanic forcing induced large discharges from the upper circulation zone and contributed significantly to the total SGD. In Case 3 where waves alone provided the forcing, the wave-induced seawater recirculation constituted 49% of the total SGD, comparable to the contribution by the tidal forcing (40%, which is slightly less than that calculated by *Robinson et al*. [2007a], possibly due to the seepage face included in the present model). When wave and tide acted together (Case 4), this portion increased to 61%. The combined effect of the two forces was not simple addition but with modulation. Nevertheless, the combined forcing further enhanced the exchange across the beach surface. The oceanic oscillations also increased the discharge associated with the density-driven circulation. This effect is likely to be related to the influence of the USP on the saltwater wedge as well as the increased mixing in the dispersion zone of the wedge under oceanic forcing [*Cooper*, 1959; *Robinson et al*., 2007a].

Total fluxes integrated across the beach zone were also calculated over the tidal cycle (Figs. 14 and 15). While both inflow and outflow could occur simultaneously at different locations across the beach, the total flux integrated over the entire beach zone had a principal direction: influx dominated between mid and high tides, and efflux for the remainder of the tidal period. The period over which efflux from the beach dominated was greater than the influx period. This asymmetry is consistent with the net outflow given by the freshwater discharge. Again the enhancement of the exchange provided by the combined forcing is clearly evident.

4. Conclusions

High frequency waves are an important and common oceanic forcing on coastal environments. Despite previous studies on wave-induced beach groundwater flow, the influence of waves on the behavior of subterranean estuaries is not well understood. Difficulties with measurements of high frequency signals hinder to some extent field investigations on wave effects and underlying processes. Similarly, numerical simulations of the system are challenged by enormous computational costs to resolve the high frequency oscillations, especially when the low frequency tide is also involved. In this study, we coupled two existing models to simulate the variably-saturated, variable-density flow in a subterranean estuary subjected to wave forcing alone and in combination with tide. A phase-averaged approach was introduced to facilitate the simulations with the combined wave and tidal forcing.

The simulation results showed that waves induced an onshore upward tilt in the phase-averaged sea level (wave set-up) and the resulting hydraulic gradient generated pore water circulations in the near-shore zone of the subterranean estuary. The circulations led to an upper saline plume similar to that due to tides. However, mixing of recirculating seawater in the USP with underlying fresh groundwater was much less intensive under the high-frequency wave oscillations compared with tidal fluctuations. Comparison between the phase-resolving and phase-averaged simulations demonstrated that the wave effect on the subterranean estuary was predominantly controlled by wave set-up, which was well represented by the phase-averaged approach. High frequency wave-induced flow oscillations simulated with the phase-resolving approach did not significantly change the mean flow or the salt-freshwater mixing. Therefore, the phase-averaged approach was adequate for simulations of the wave effects on the near-shore groundwater flow and transport processes.

In the case of combined forcing, wave-induced circulations coupled with the intra-tidal flows strengthened the averaged, circulating flows over the tidal period. These circulations increased exchange between the subterranean estuary and ocean, contributing 61% of the total submarine groundwater discharge for the simulated condition in comparison with the 40% and 49% proportions caused by individual tidal and wave forcing, respectively. The combined forces also created a more extensive USP with the freshwater discharge zone shifted further seaward. The freshwater flow paths in the intertidal subterranean estuary were altered with a significant increase in the associated transit times. The interplay of waves and tides led to intensified mixing between discharging fresh groundwater and recirculating seawater. These results demonstrate further the complexity of near-shore groundwater systems subjected to oceanic forcing and indicate the need to consider dynamic forcing including waves in studies of the fate of chemicals in subterranean estuaries.

The study has assumed a constant incoming wave condition over a semi-diurnal tide. In reality, both wave height and period tend to vary with time randomly, following certain statistical distributions. Such random waves are likely to induce pore water flow oscillations of periods longer than the primary wave period, which in turn may modify the circulating flows in the USP and lower saltwater wedge, and increase salt-freshwater mixing. The model also assumed a homogeneous, isotropic subterranean estuary. Heterogeneity would complicate further the flow and transport processes. Other factors that are likely to influence how the subterranean estuary responds to oceanic forcing include irregular beach morphology, multiple tidal constituents (e.g., spring-neap tides), long period sea level oscillations, and seasonal variations of the inland hydraulic head and freshwater discharge. All these gaps point to directions for further studies on the dynamics of the subterranean estuary. This work, having shed light on the wave effect with and without the tidal modulation, provides a sound basis for these future studies.

Acknowledgments

This research has been supported by an ARC Discovery Grant (DP0988718). CR acknowledges NSERC Discovery Grant (386448-2010). DAB and RB acknowledge SNF (200021_124780). The authors acknowledge valuable comments from three anonymous reviewers, which have led to improvement of the paper.

References

Anschutz, P., T. Smith, A. Mouret, J. Deborde, S. Bujan, D. Poirier and P. Lecroart (2009), Tidal sands as biogeochemical reactors, *Estuarine, Coastal and Shelf Science, 84*(1), 84-90.

Bakhtyar, R., A. Brovelli, D. A. Barry, and L. Li (2010), Wave-induced watertable fluctuations, sediment transport and beach profile change: Modeling and comparison with large-scale laboratory experiments, *Coastal Engineering*, doi: 10.1016/j.coastaleng.2010.08.004, in press.

Boufadel, M. C. (2000), A mechanistic study of nonlinear solute transport in a groundwater-surface water system under steady state and transient hydraulic conditions, *Water Resources Research, 36*(9), 2549-2565.

Brovelli, A., X. Mao, and D. A. Barry (2007), Numerical modeling of tidal influence on density-dependent contaminant transport, *Water Resources Research*, *43*(10), W10426, doi:10.1029/2006WR005173.

Cartwright, N., L. Li and P. Nielsen (2004), Response of the salt-freshwater interface in a coastal aquifer to a wave-induced groundwater pulse: Field observations and modelling, *Advances in Water Resources*, *27*(3), 297-303.

Carsel, R. F. and R. S. Parrish (1988), Developing joint probability distributions of soil water retention characteristics, *Water Resources Research*, *24*(5), 755-769.

Colbert, S. L., W. M. Berelson, and D. E. Hammond (2008), Radon-222 budget in Catalina Harbor, California: 2. Flow dynamics and residence time in a tidal beach, *Limnology and Oceanography*, *53*(2), 659-665.

Cooper, H. H. (1959), A hypothesis concerning the dynamic balance of fresh water and salt water in a coastal aquifer, *Journal of Geophysical Research*, *64*(4), 461-467.

Gardner, L. R., and A. M. Wilson (2006), Comparison of four numerical models for simulating seepage from salt marsh sediments, *Estuarine, Coastal and Shelf Science*, *69*(3-4), 427-437.

Fischer, H. B., E. J. List, R. Koh, J. Imberger and N. Brooks (1979), *Mixing in Inland and Coastal Waters*, Academic, San Diego, California, USA.

Hibberd, S., and D. H. Peregrine (1979), Surf and run-up on a beach: A uniform bore, *Journal of Fluid Mechanics*, *95*, 323-345.

Horn D. (2006), Measurements and modelling of beach groundwater flow in the swash-zone: a review, *Continental Shelf Research*, *26*(5), 622-652.

Kobayashi, N., K. O. Ashwini and I. Roy (1987), Wave reflection and run-up on rough slopes, *Journal of Waterway, Port, Coastal, and Ocean Engineering*, *113*(3), 282-298.

Li, L., D. A. Barry, F. Stagnitti and J. Y. Parlange (1999), Submarine groundwater discharge and associated chemical input to a coastal sea, *Water Resources Research, 35*(11), 3253-3259.

Li, L., and D. A. Barry (2000), Wave-induced beach groundwater flow, *Advances in Water Resources*, *23*(4), 325-337.

Li., L., D. A. Barry, C. B. Pattiaratchi, and G. Masselink (2002), BeachWin: Modelling groundwater effects on swash sediment transport and beach profile changes, *Environmental Modelling and Software*, 17(3), 313-320.

Li, H. L., M. C. Boufadel, and J. W. Weaver (2008), Tide-induced seawater-groundwater circulation in shallow beach aquifers, *Journal of Hydrology, 352*(1-2): 211-224.

Li, X., B. X. Hu, W. C. Burnett, I. R. Santos, and J. P. Chanton (2009), Submarine ground water discharge driven by tidal pumping in a heterogeneous aquifer, *Ground Water*, *47*(4), 558-568.

Longuet-Higgins, M. S. (1983), Wave set-up, percolation and undertow in the surf zone, Proceedings of the Royal Society of London, Series A, Mathematical and Physical, 390 (1799), 283-291.

Mao, X., P. Enot, D. A. Barry, L. Li, A. Binley, and D. S. Jeng (2006), Tidal influence on behaviour of a coastal aquifer adjacent to a low-relief estuary, *Journal of Hydrology, 327*(1-2),110-27.

Maji R., and L. Smith (2009), Quantitative analysis of seabed mixing and intertidal zone discharge in coastal aquifers, *Water Resources Research, 45*(11), W11401, doi:10.1029/2008WR007532.

Martínez, M. L., A. Intralawan, G. Vázquez, O. Pérez-Maqueo, P. Sutton, and R. Landgrave (2007), The coasts of our world: Ecological, economic and social importance, *Ecological Economics*, *63*(2-3), 254-272.

Moore, W. S. (1996), Large groundwater inputs to coastal waters revealed by Ra-226 enrichments, *Nature*, *380*(6575), 612-614.

Moore, W. S. (1999), The subterranean estuary: A reaction zone of ground water and sea water, *Marine Chemistry, 65*(1-2), 111-125.

Moore, W. S. (2010), The effect of submarine groundwater discharge on the ocean, *Annual Review of Marine Science*, *2*: 59-88.

Nielsen, P. (1999), Groundwater dynamics and salinity in coastal barriers, *Journal of Coastal Research*, *15*(3), 732-740.

Prieto, C., and G. Destouni (2005), Quantifying hydrological and tidal influences on groundwater discharges to coastal waters, *Water Resources Research, 41*(12), W12427. doi:20.1029/

2004WR003920.

Reeves, H. W., P. M. Thibodeau, R. G. Underwood, and L. R. Gardner (2000), Incorporation of total stress changes into the groundwater model SUTRA, *Ground Water, 38*(1), 88-99.

Robinson, C., and L. Li (2004), Effect of tidal oscillations on water exchange and mixing in a coastal aquifer, *15th International Conference on Computational Methods in Water Resources*, Chapel Hill, North Carolina, USA.

Robinson, C., B. Gibbes, and L. Li (2006), Driving mechanisms for flow and salt transport in a subterranean estuary, *Geophysical Research Letters, 33*(3), L03402, doi:10.1029/2005GL025247.

Robinson, C., L. Li, and D. A. Barry (2007a), Effect of tidal forcing on a subterranean estuary, *Advances in Water Resources, 30*(4), 851-865.

Robinson, C., L. Li, and H. Prommer (2007b), Tide-induced recirculation across the aquifer-ocean interface, *Water Resources Research, 43*(7), W07428, doi:10.1029/2006WR005679.

Robinson, C., A. Brovelli, D. A. Barry, and L. Li (2009), Tidal influence on BTEX biodegradation in sandy coastal aquifers, *Advances in Water Resources*. *32*(1): 16-28.

Smith, A. J., L. R. Townley, and M. G. Trefry (2005), Visualization of aquifer response to periodic forcing, *Advances in Water Resources, 28*(8), 819-834.

Sorenson, R. M. (2006), *Basic Coastal Engineering*, Third Edition, Springer, New York, USA.

Taniguchi, M., W. C. Burnett, J. E. Cable, and J. V. Turner (2002), Investigation of submarine groundwater discharge, *Hydrological Processes*, *16*(11), 2115-2129.

Turner, I. L., B. P. Coates, and R. I. Acworth (1997), Tides, waves and the super-elevation of groundwater at the coast, *Journal of Coastal Research*, *13*(1), 46-60.

van Genuchten, M. T. (1980), A closed form equation for predicting the hydraulic conductivity of unsaturated soils. *Soil Science Society of America Journal*, *44*(5), 892-898.

Vandenbohede, A., and L. Lebbe (2005), Occurrence of salt water above fresh water in dynamic equilibrium in a coastal groundwater flow system near De Panne, Belgium, *Hydrogeology Journal*, *14*(4), 462-472.

Voss, C. I., and A. M. Provost (2002), *A model for saturated-unsaturated, variable-density ground-water flow with solute or energy transport*, U.S. Geological Survey. Water-Resources Investigations Report, 02-4231, Reston, Virginia, USA.

Xin, P., G. Jin, L. Li, and D. A. Barry (2009), Effects of crab burrows on pore water flows in salt marshes, *Advances in Water Resources*, *32*(3), 439-449.

Younger, P. L. (1996), Submarine groundwater discharge, *Nature*, *382*(6587), 121-122.

Zimmerman J. T. F. (1976), Mixing and flushing of tidal embayments in the western Dutch Wadden Sea part I: Distribution of salinity and calculation of mixing time scales, *Netherlands Journal of Sea Research 10*(2), 149-191.

Notation

A	amplitude [L]
C	salt concentration [-]
C^*	salt concentration of the fluid source [-]
$\mathbf{D}$	hydrodynamic dispersion tensor [L^2T^{-1}]
g	magnitude of the gravitational acceleration [LT^{-2}]
H	deep water sea level [L]
h	water depth [L]
K_S	saturated hydraulic conductivity [LT^{-1}]
$K(\psi)$	hydraulic conductivity [LT^{-1}]
n	*van Genuchten* constant for water retention curve [-]
P	pore water pressure [$ML^{-1}T^{-2}$]
Q	fluid source [L^3T^{-1}]
Q_d	density-driven flow discharge per unit width [L^2T^{-1}]
Q_f	terrestrially derived fresh water discharge per unit width [L^2T^{-1}]
Q_t	tidally-driven flow discharge per unit width [L^2T^{-1}]
Q_w	wave-induced flow discharge per unit width [L^2T^{-1}]
$\vec{q}$	Darcy flux [LT^{-1}]
S_W	water saturation [-]
S_{Wres}	residual water saturation [-]
T	period [T]
t	time [T]
u	depth-averaged flow velocity [LT^{-1}]
x	horizontal coordinate [L]
z	elevation [L]
Z_{MSL}	mean sea level [L]
α	*van Genuchten* constant for water retention curve [L^{-1}]
α_L	longitudinal dispersivity [L]
α_T	transverse dispersivity [L]
γ	beach angle [-]
ω	angular frequency [T^{-1}]

ϕ	soil porosity [-]
ρ	fluid density [ML^{-3}]
ρ_0	freshwater density [ML^{-3}]
ρ_s	density of fluid source [ML^{-3}]
ψ	capillary pressure head [L]

List of figures

Fig. 1 Conceptual diagram of a subterranean estuary including major near-shore flow processes (after *Robinson et al*. [2007a]): (1) density-driven circulation, (2) tide-induced circulation, (3) circulation driven by wave set-up and (4) inland fresh groundwater discharge. The landward boundary of the subterranean estuary is defined by the characteristic length of tidal wave propagation in the aquifer. Boundary **ABCDEF** represents the model domain.

Fig. 2 Simulated flow fields during wave run-up (a, elapsed time 0 s; b, elapsed time 2.5 s) and run-down (c, elapsed time 5 s; d, elapsed time 7.5 s). Salt concentrations (in ppt) are also given in the figure. (e) and (f) are enlarged figures for the wave-front shown in (c) and (d), respectively.

Fig. 3 (a) Comparison between the averaged flow field given by the phase-resolving simulation (white arrows) and the flow field predicted with the phase-averaged approach (black arrows). Salt concentrations from the phase-averaged simulation (in ppt) are also shown. The dotted line indicates the phase-averaged nearshore sea water surface. (b) Change of the upper saline plume and the saltwater wedge (indicated by arrows) from the phase-averaged simulation result (thin lines) to the phase-resolving simulation result (thick lines). Contours of 90% and 10% of the seawater salt concentration are shown.

Fig. 4 Salt concentrations (in ppt) and particle path lines for Case 1 (static). Numbers at the path lines indicate the travel times in days. The dotted line indicates the coastal water level.

Fig. 5 Salt concentrations (in ppt) and particle path lines at the quasi-steady state (based on phase-averaged flow) for Case 2 (tide). Numbers at the path lines indicate the travel times in days. The two dotted lines indicate the extent of the intertidal zone.

Fig. 6 Salt concentrations (in ppt) and particle path lines (based on the phase-averaged simulation) for the Case 3 (wave). Numbers at the path lines indicate the travel times in days. The dotted line indicates the averaged sea level.

Fig. 7 Phase-averaged hydraulic heads at the beach surface for Case 2 (dashed line), Case 3 (triangles) and Case 4 (circles). The solid line shows the beach surface. The arrow indicates the wave-breaking point.

Fig. 8 Variations of pore water velocities with time. (a) for the dynamic wave. The observation point is at the center of the USP (x = -1 m and z = -5 m); (b) for the tide. The observation point is at the center of the USP (x = 0 m and z = -7 m).

Fig. 9 Simulated flow fields for Case 4 at the rising tide (a, elapsed time 0 h), high tide (b, elapsed time 3 h), falling tide (c, elapsed time 6 h) and low tide (d, elapsed time 9 h). For comparison, the flow fields for Case 2 are given in Figures e-h. The dashed line indicates the sea level.

Fig. 10 (a) Salt concentrations (in ppt) and particle path lines (based on phase-averaged flow) for Case 4 (combined wave and tide). Numbers at path lines indicate the travel times in days. The two dotted lines indicate the extent of the intertidal zone, affected by wave action.

Fig. 11 Particle paths calculated using the phase-averaged flow field (solid line) and instantaneous flow field (circles). (a) for the tide (particle initially placed at x = 0 m and z = -7 m); and (b) is for the dynamic wave (particle initially placed at x = -1 m and z = -5 m).

Fig. 12 Net water influx and efflux rates per unit width along the aquifer-ocean interface. (a), static; (b), wave; (c) tide and (d), combined wave and tide. FD is the freshwater discharge zone.

Fig. 13 Net salt influx and efflux rates per unit width along the aquifer-ocean interface. (a), static; (b), wave; (c) tide and (d), combined wave and tide. FD is the freshwater discharge zone.

Fig. 14 Temporal variations of the water discharge per unit width along the aquifer-ocean interface.

Fig. 15 Temporal variations of the salt flux per unit width along the aquifer-ocean interface.

Table 1. Coordinates of reference points of the model domain (*x*, *z*).

A (m)	**B** (m)	**C** (m)	**D** (m)	**E** (m)	**F** (m)
(-150, 3)	(-150, -30)	(50, -30)	(50, -3)	(30, -3)	(-30, 3)

Table 2. Calculated water discharge and recirculation rates across the aquifer-ocean interface (per unit width of shoreline). WTDC represents the circulation driven by wave and/or tide. DDC represents the density-driven circulation.

Case		Static	Tide	Wave		Wave combined tide
				Phase-resolving	Phase-averaged	
SGD (m^3/d)		2.30	5.54	5.28	4.56	7.42
Circulation rate (m^3/d)	WTDC	0	2.21	2.53	2.23	4.49
	DDC	0.20	1.22	0.65	0.23	0.82
Circulation percent (%)	WTDC	0	40	48	49	61
	DDC	9	22	12	5	11

732

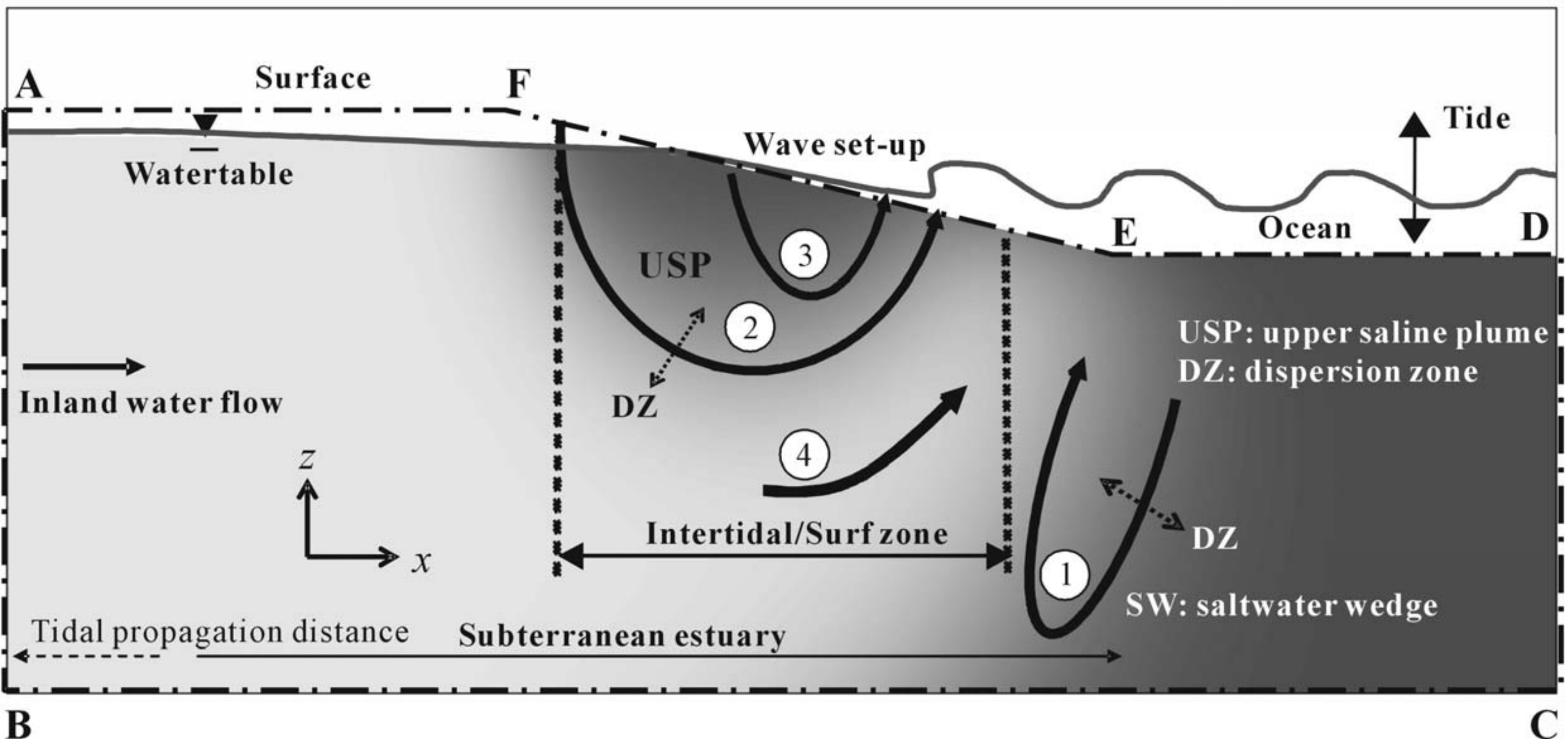

A
Surface
F
Watertable
Wave set-up
Tide
E
Ocean
D
USP
3
2
USP: upper saline plume
DZ: dispersion zone
Inland water flow
DZ
4
z
x
Intertidal/Surf zone
DZ
1
SW: saltwater wedge
Tidal propagation distance
Subterranean estuary
B
C

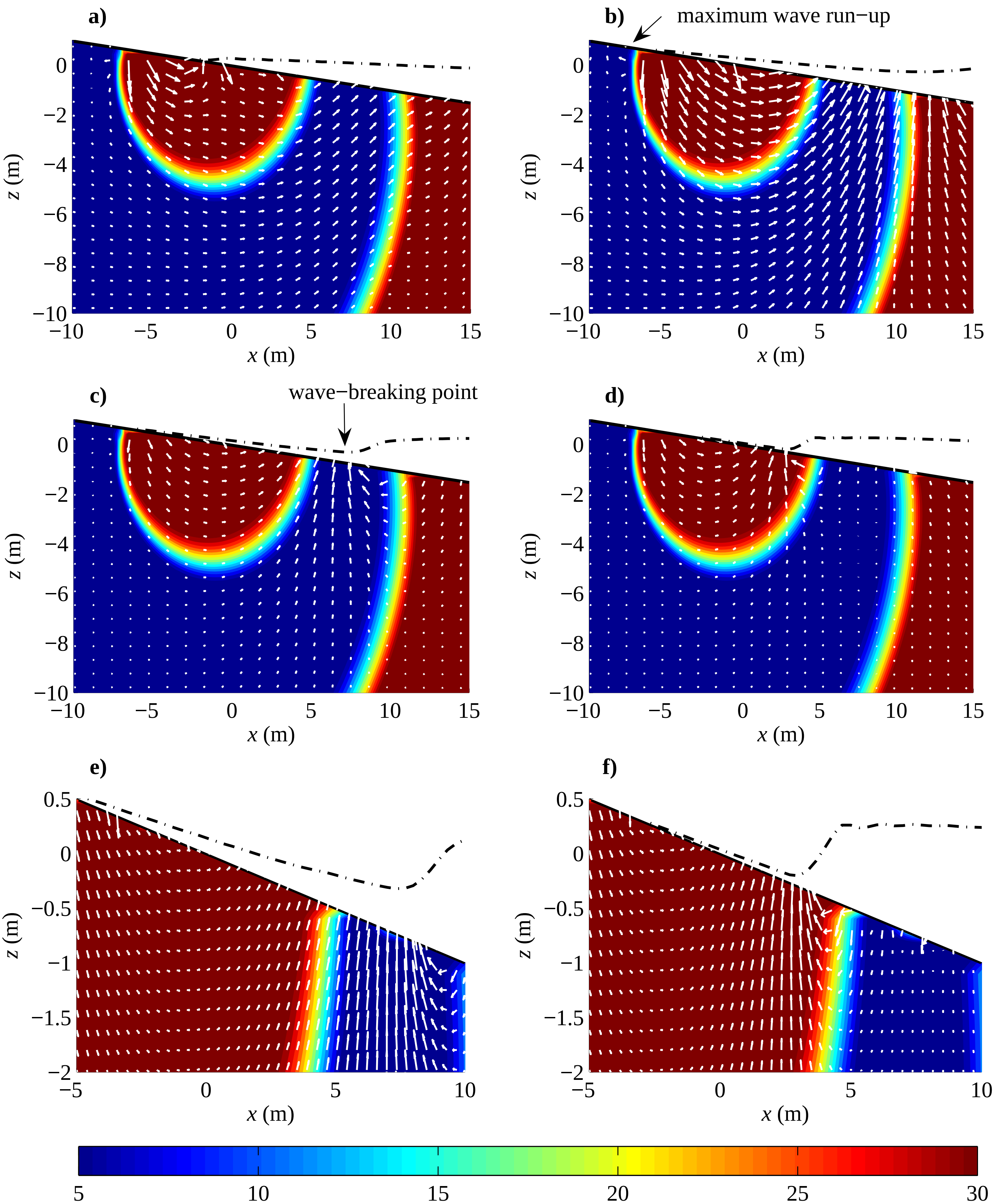

a)
b)
maximum wave run−up
c)
wave−breaking point
d)
e)
f)
z (m)
x (m)
0
−2
−4
−6
−8
−10
−10
−5
0
5
10
15
0.5
−0.5
−1
−1.5
−2
5
10
15
20
25
30

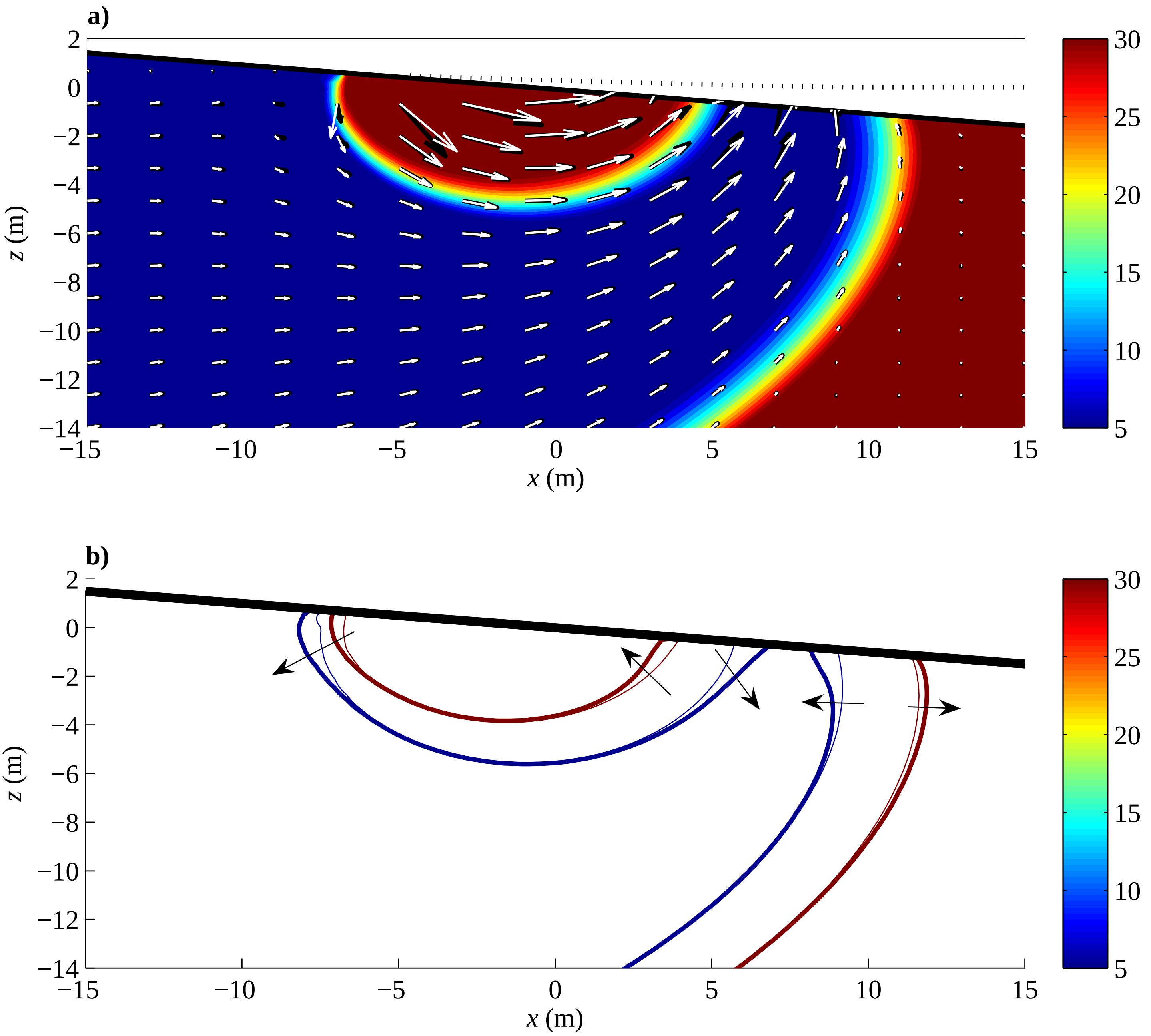

a)
b)
z (m)
x (m)
2
0
−2
−4
−6
−8
−10
−12
−14
−15
−10
−5
0
5
10
15
30
25
20
15
10
5

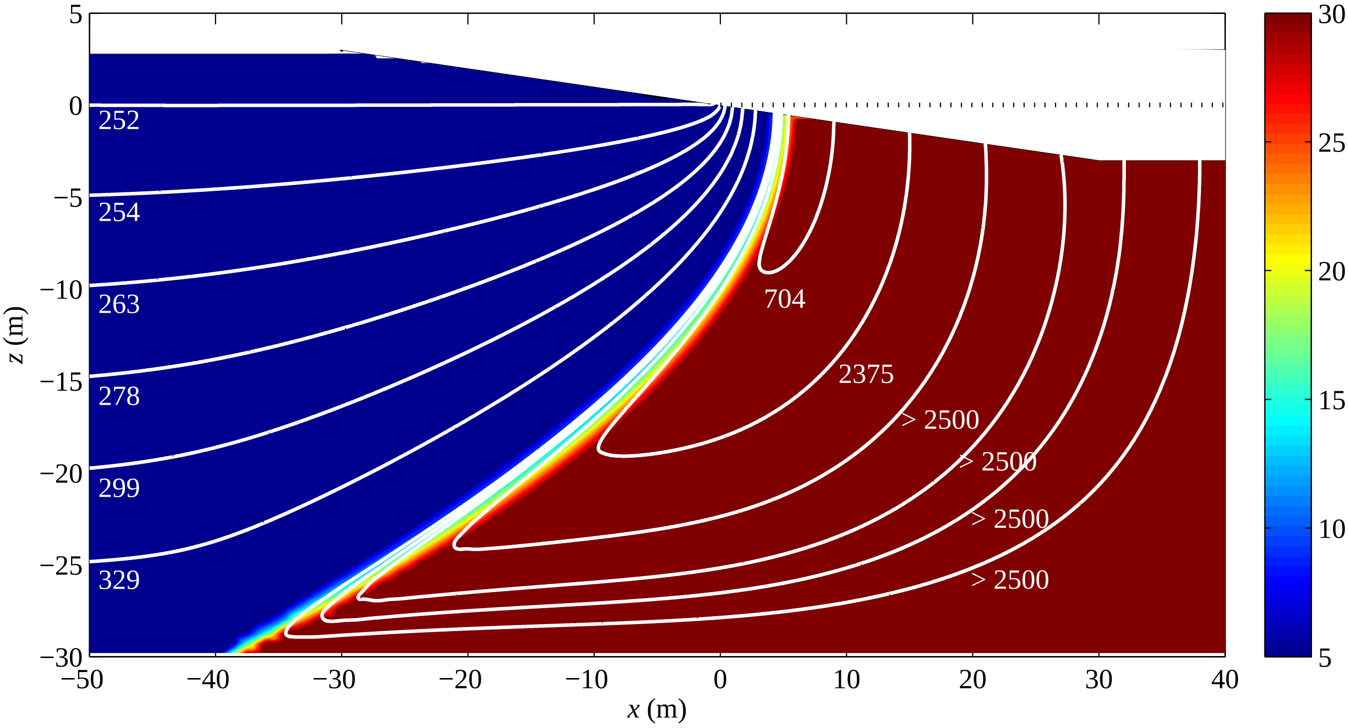

252
254
263
278
299
329
704
2375
> 2500
> 2500
> 2500
> 2500
z (m)
x (m)
5
0
−5
−10
−15
−20
−25
−30
−50
−40
−30
−20
−10
0
10
20
30
40
30
25
20
15
10
5

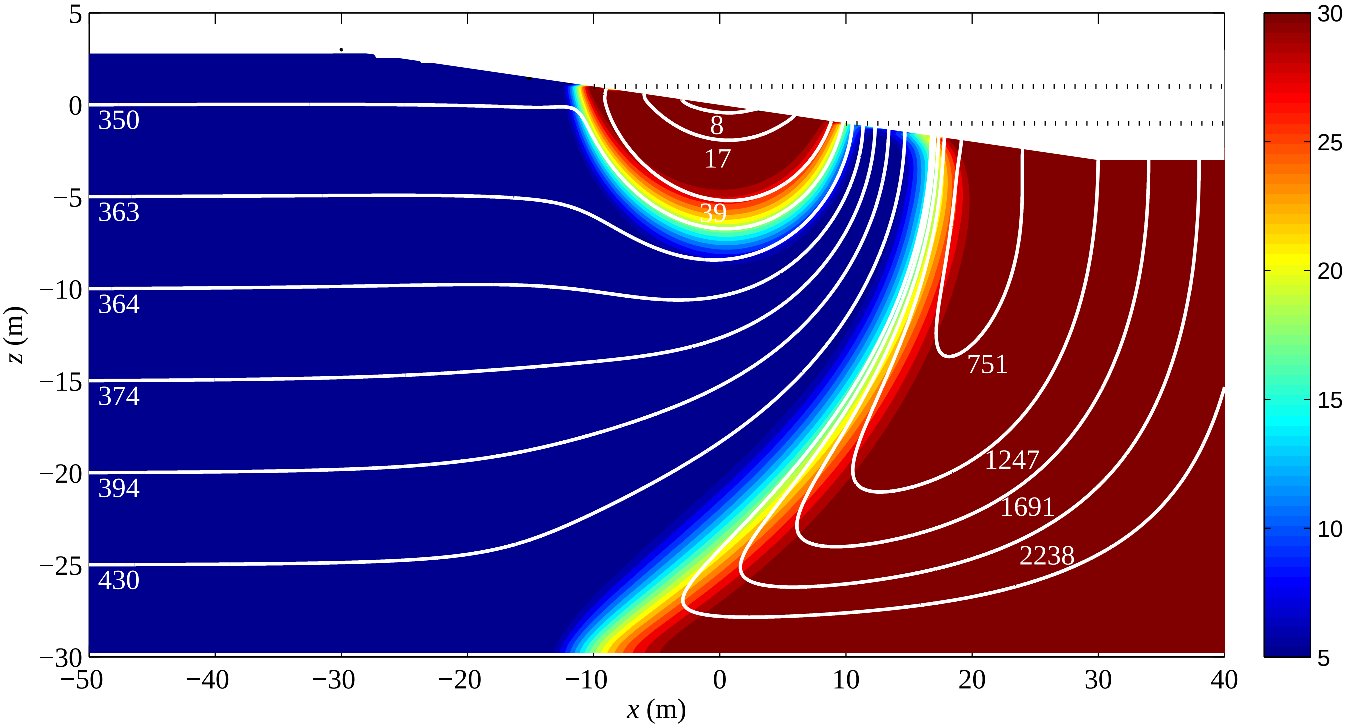

5
0
−5
−10
−15
−20
−25
−30
z (m)
−50
−40
−30
−20
−10
0
10
20
30
40
x (m)
350
363
364
374
394
430
8
17
39
751
1247
1691
2238
30
25
20
15
10
5

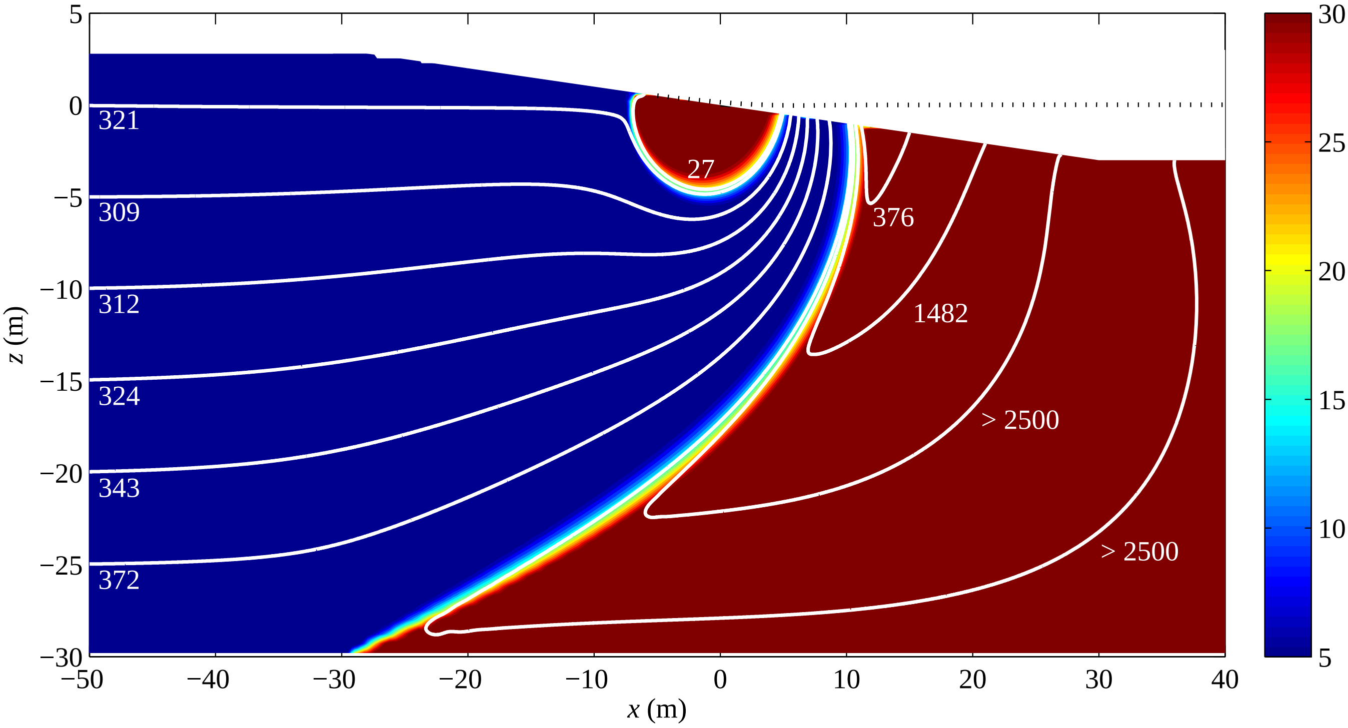

5
0
−5
−10
−15
−20
−25
−30
z (m)
−50
−40
−30
−20
−10
0
10
20
30
40
x (m)
321
309
312
324
343
372
27
376
1482
> 2500
> 2500
30
25
20
15
10
5

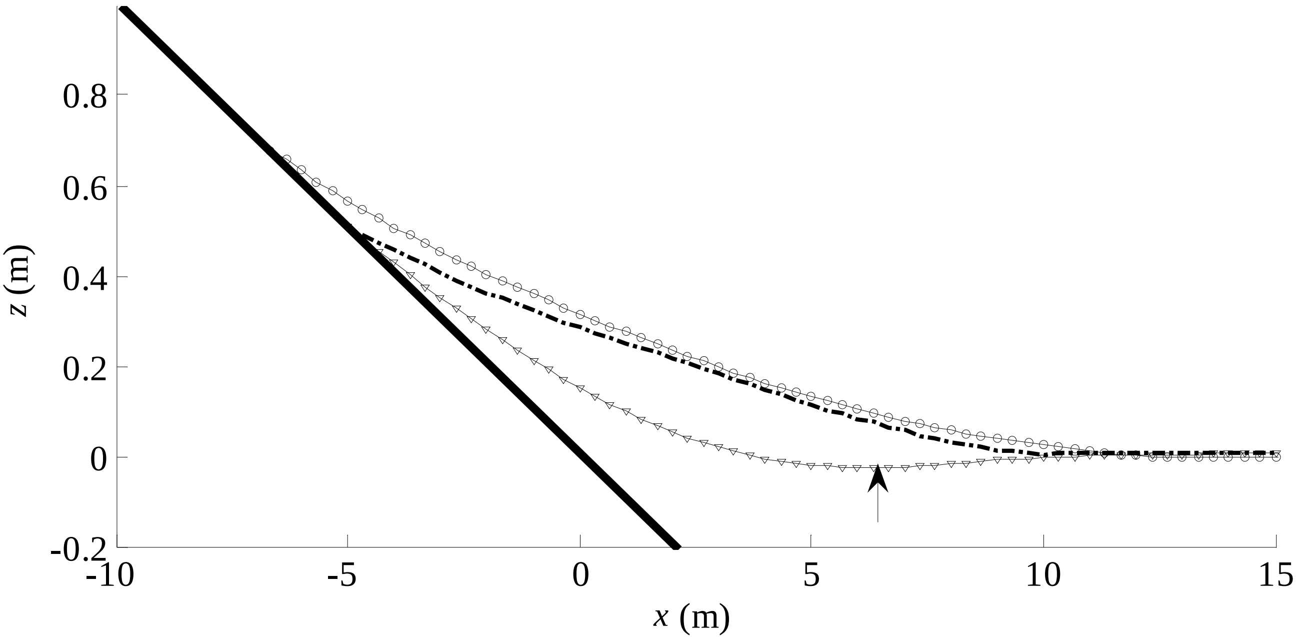

0.8
0.6
0.4
0.2
0
-0.2
z (m)
-10
-5
0
5
10
15
x (m)

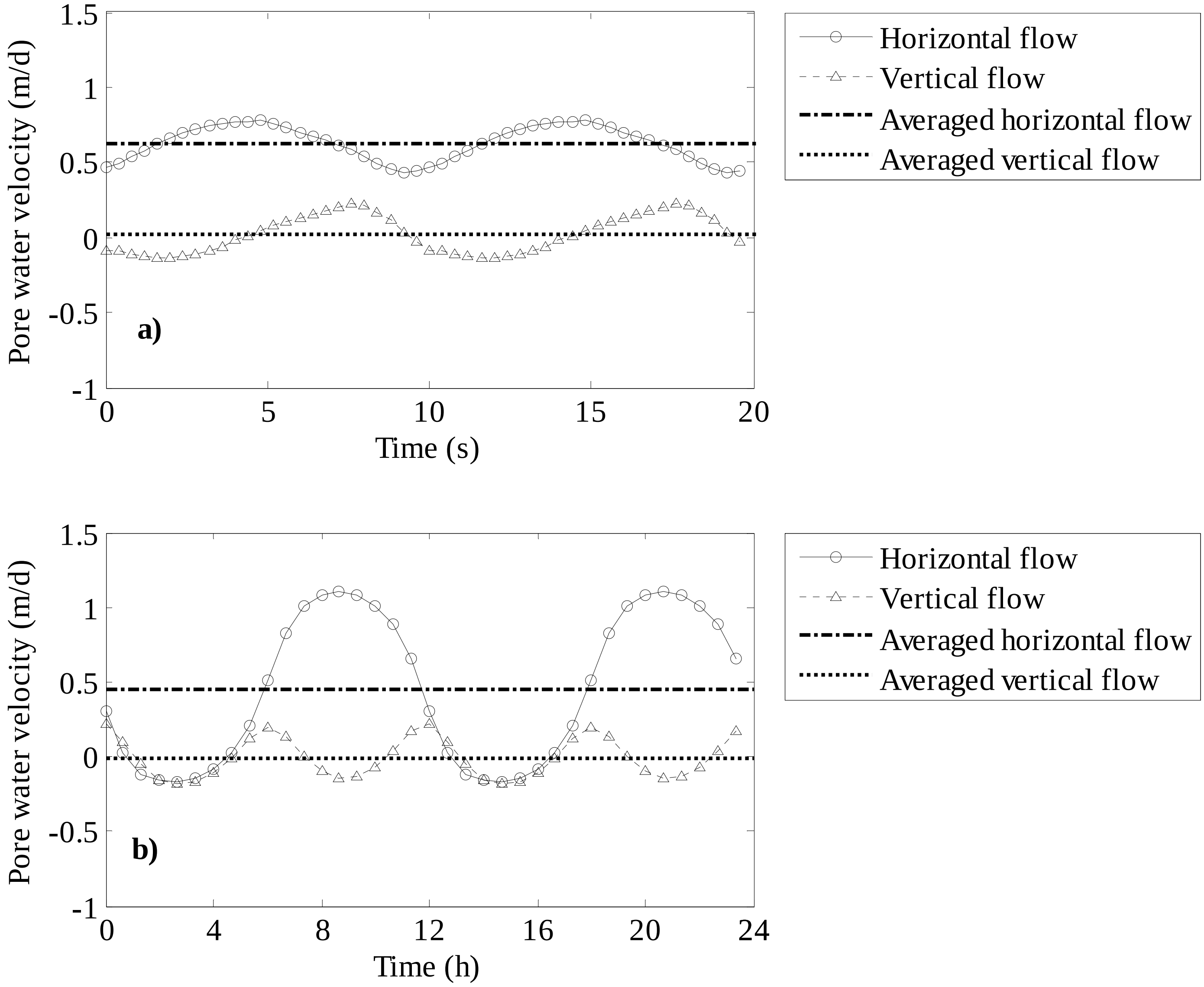

Pore water velocity (m/d)
Time (s)
a)
Horizontal flow
Vertical flow
Averaged horizontal flow
Averaged vertical flow
Pore water velocity (m/d)
Time (h)
b)
Horizontal flow
Vertical flow
Averaged horizontal flow
Averaged vertical flow

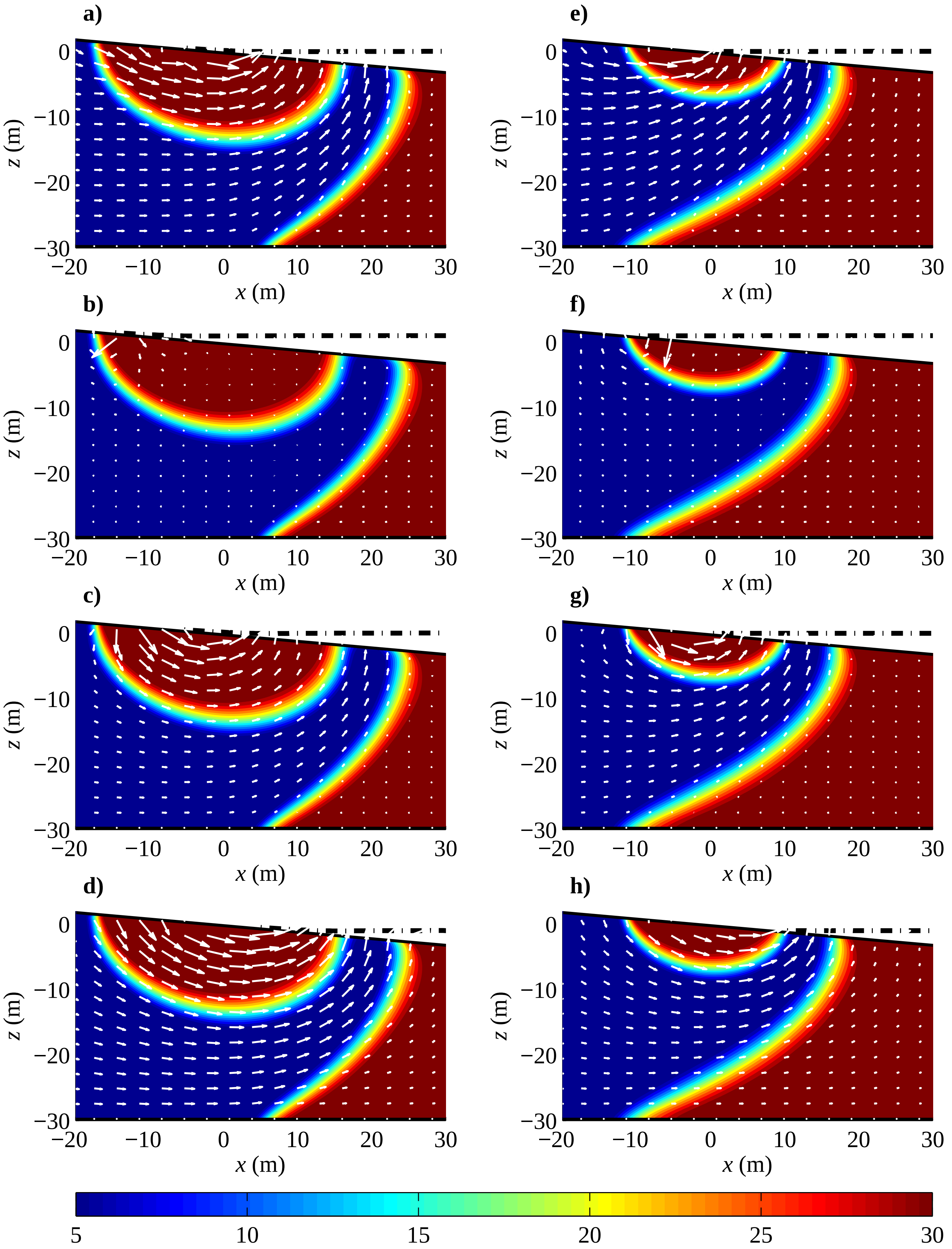

a)
b)
c)
d)
e)
f)
g)
h)
z (m)
x (m)
0
−10
−20
−30
−20
10
20
30
5
15
25

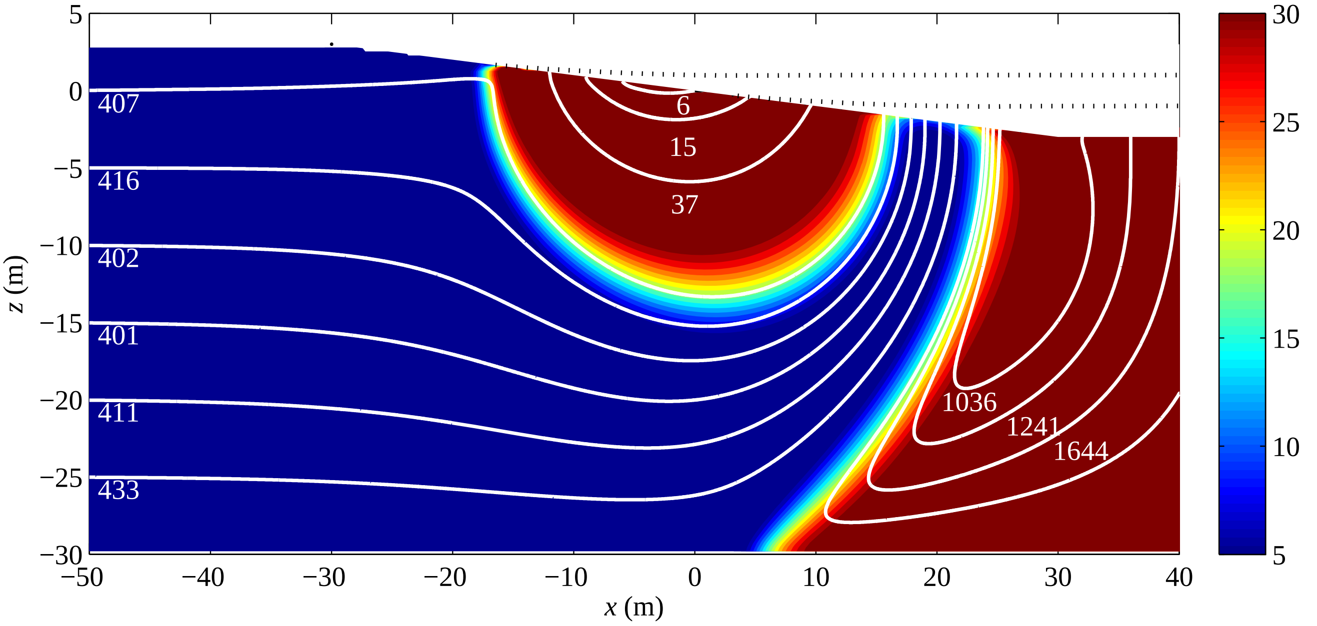

5
0
−5
−10
−15
−20
−25
−30
z (m)
−50
−40
−30
−20
−10
0
10
20
30
40
x (m)
407
416
402
401
411
433
6
15
37
1036
1241
1644
30
25
20
15
10
5

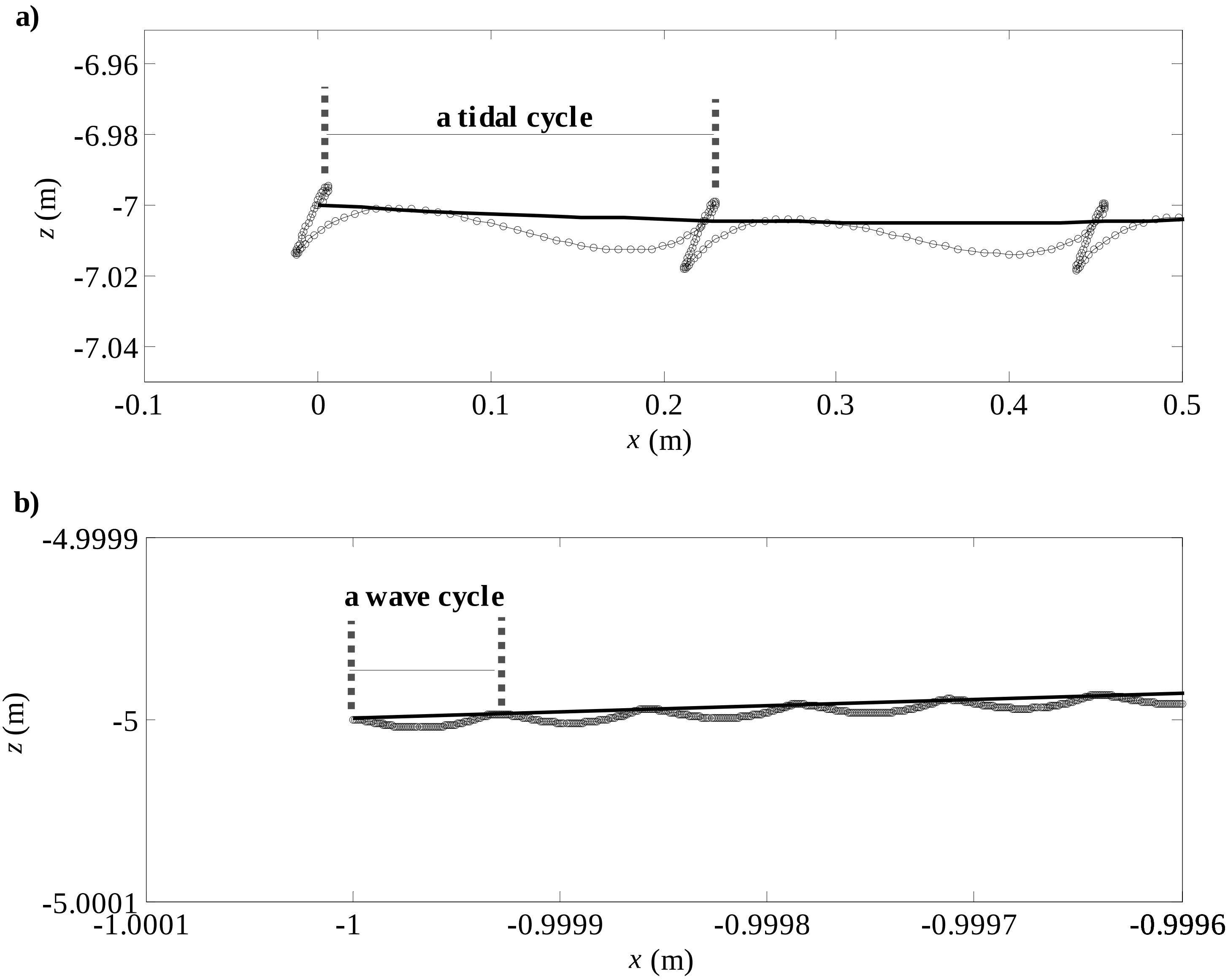

a)
a tidal cycle
-6.96
-6.98
-7
-7.02
-7.04
z (m)
-0.1
0
0.1
0.2
0.3
0.4
0.5
x (m)
b)
a wave cycle
-4.9999
-5
-5.0001
z (m)
-1.0001
-1
-0.9999
-0.9998
-0.9997
-0.9996
x (m)

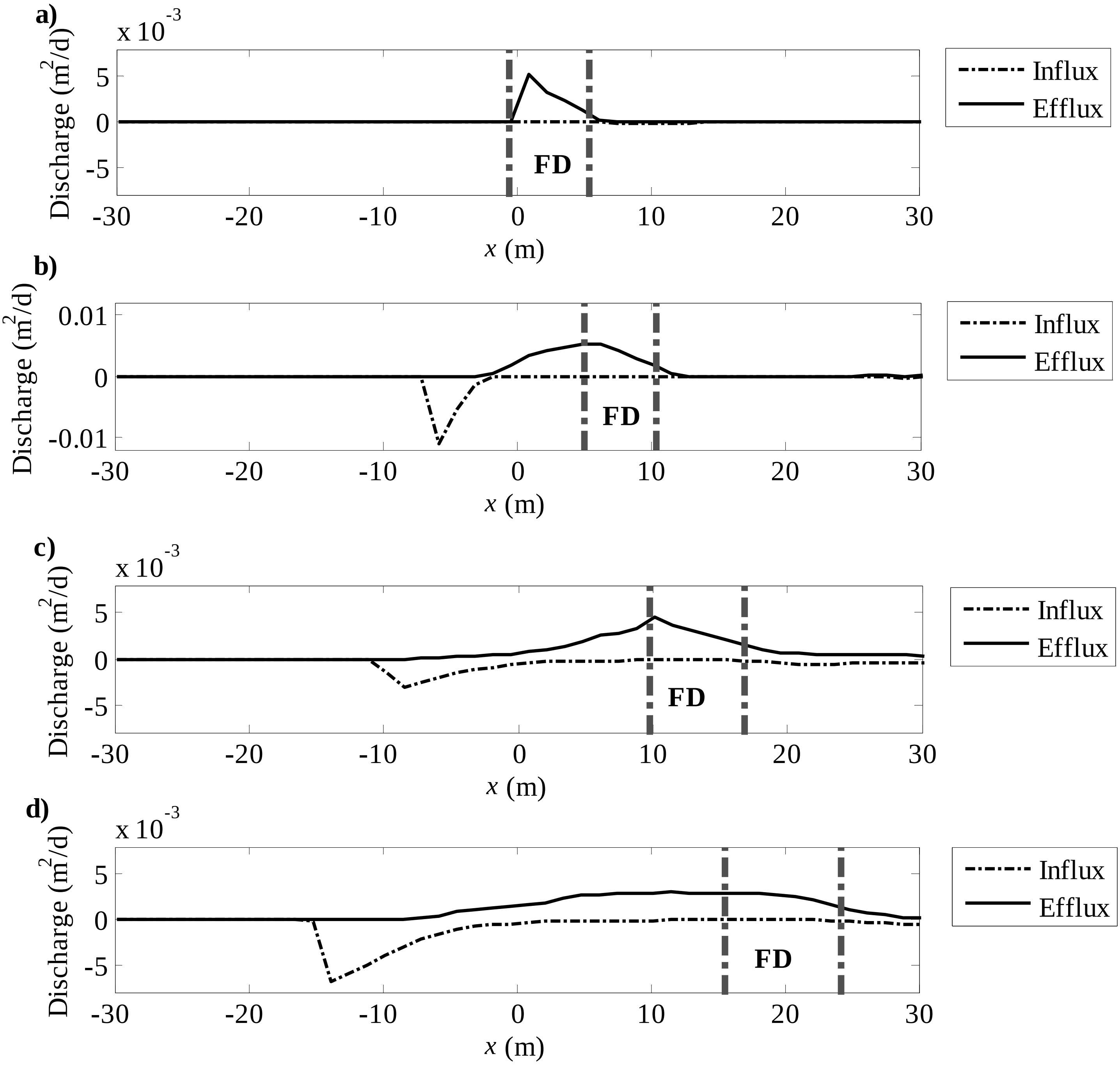
a)
x 10^-3
Discharge (m^2/d)
FD
Influx
Efflux
x (m)
b)
Discharge (m^2/d)
FD
Influx
Efflux
x (m)
c)
x 10^-3
Discharge (m^2/d)
FD
Influx
Efflux
x (m)
d)
x 10^-3
Discharge (m^2/d)
FD
Influx
Efflux
x (m)

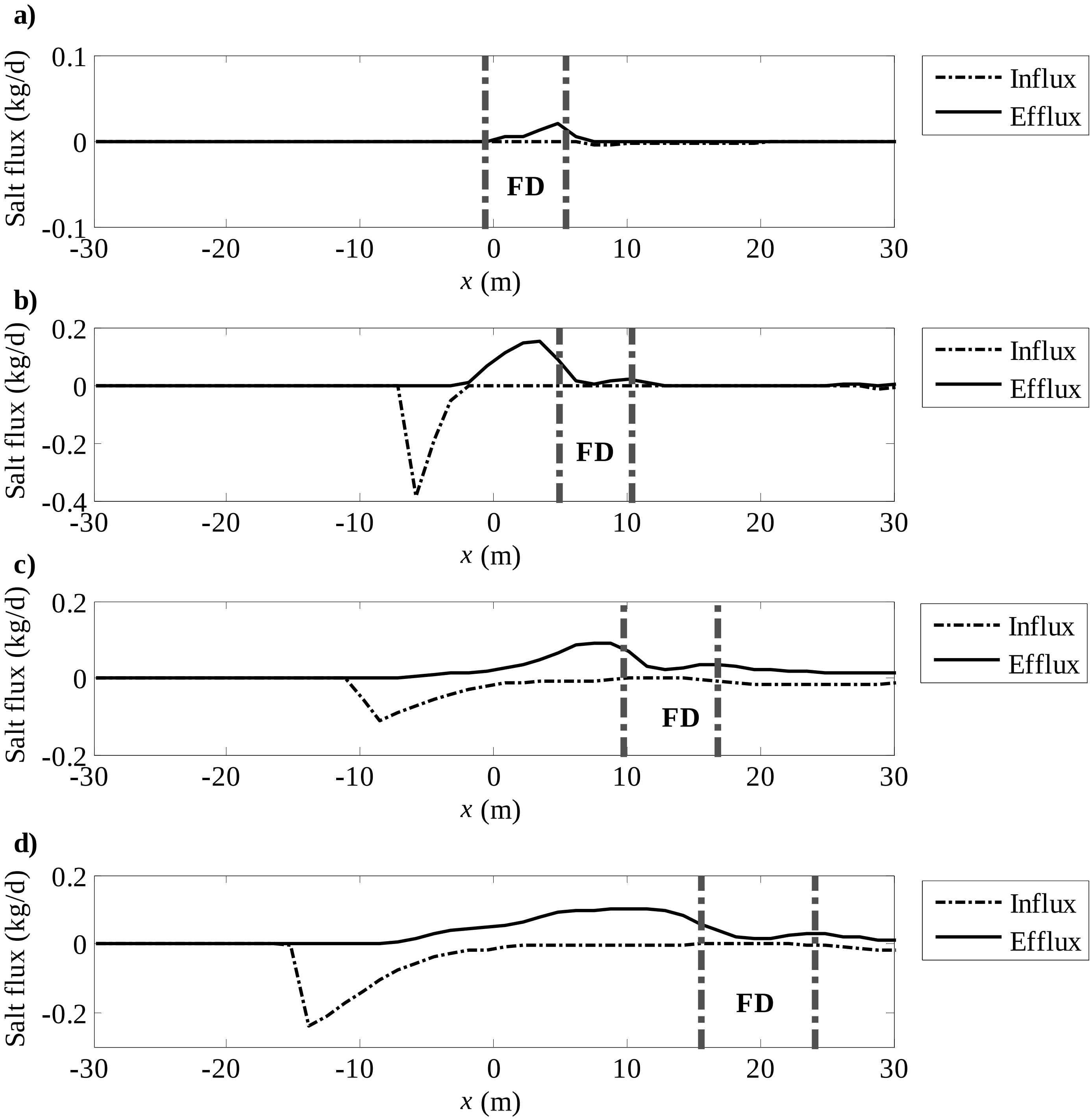
a)
Salt flux (kg/d)
0.1
0
-0.1
FD
-30
-20
-10
0
10
20
30
x (m)
Influx
Efflux
b)
Salt flux (kg/d)
0.2
0
-0.2
-0.4
FD
-30
-20
-10
0
10
20
30
x (m)
Influx
Efflux
c)
Salt flux (kg/d)
0.2
0
-0.2
FD
-30
-20
-10
0
10
20
30
x (m)
Influx
Efflux
d)
Salt flux (kg/d)
0.2
0
-0.2
FD
-30
-20
-10
0
10
20
30
x (m)
Influx
Efflux

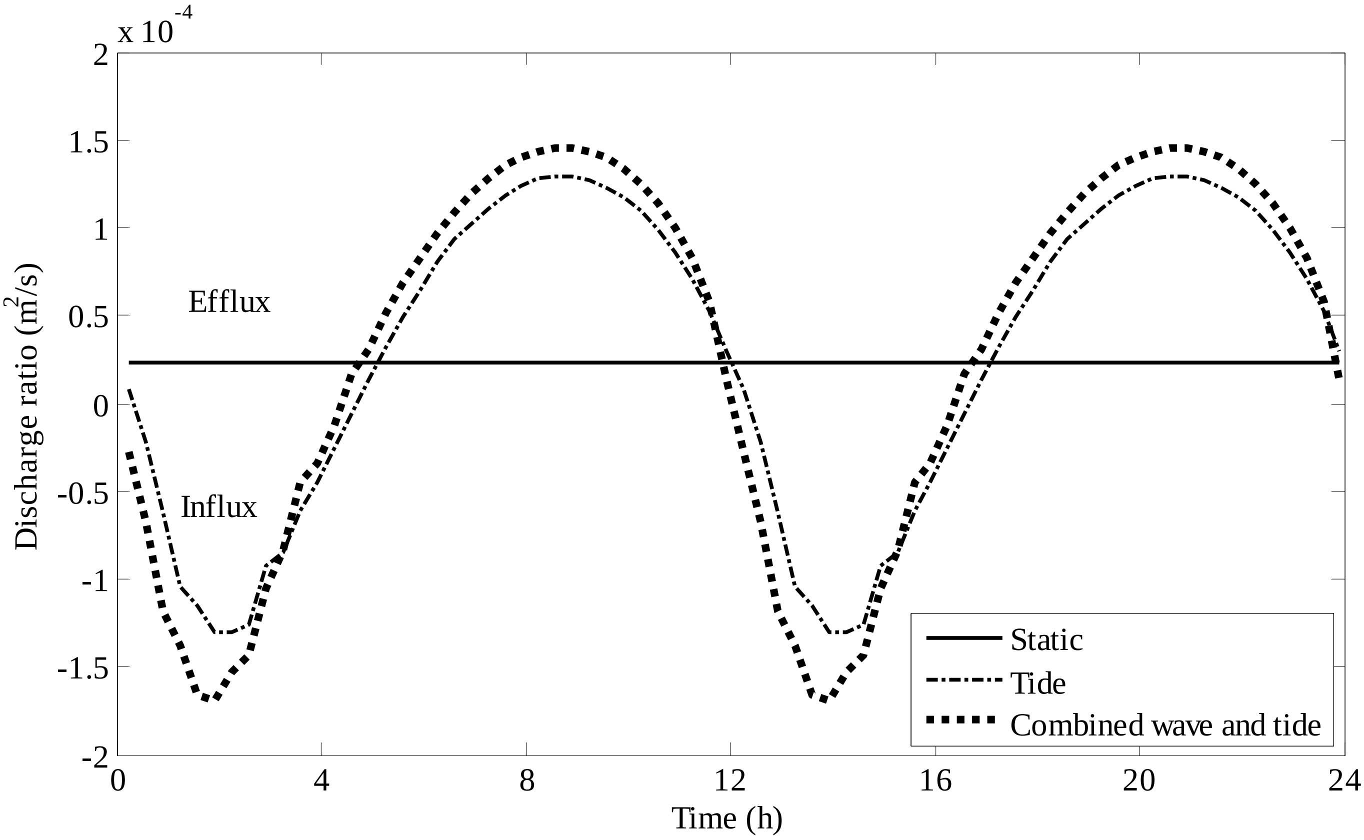

x 10^-4
Discharge ratio (m²/s)
Efflux
Influx
Static
Tide
Combined wave and tide
Time (h)

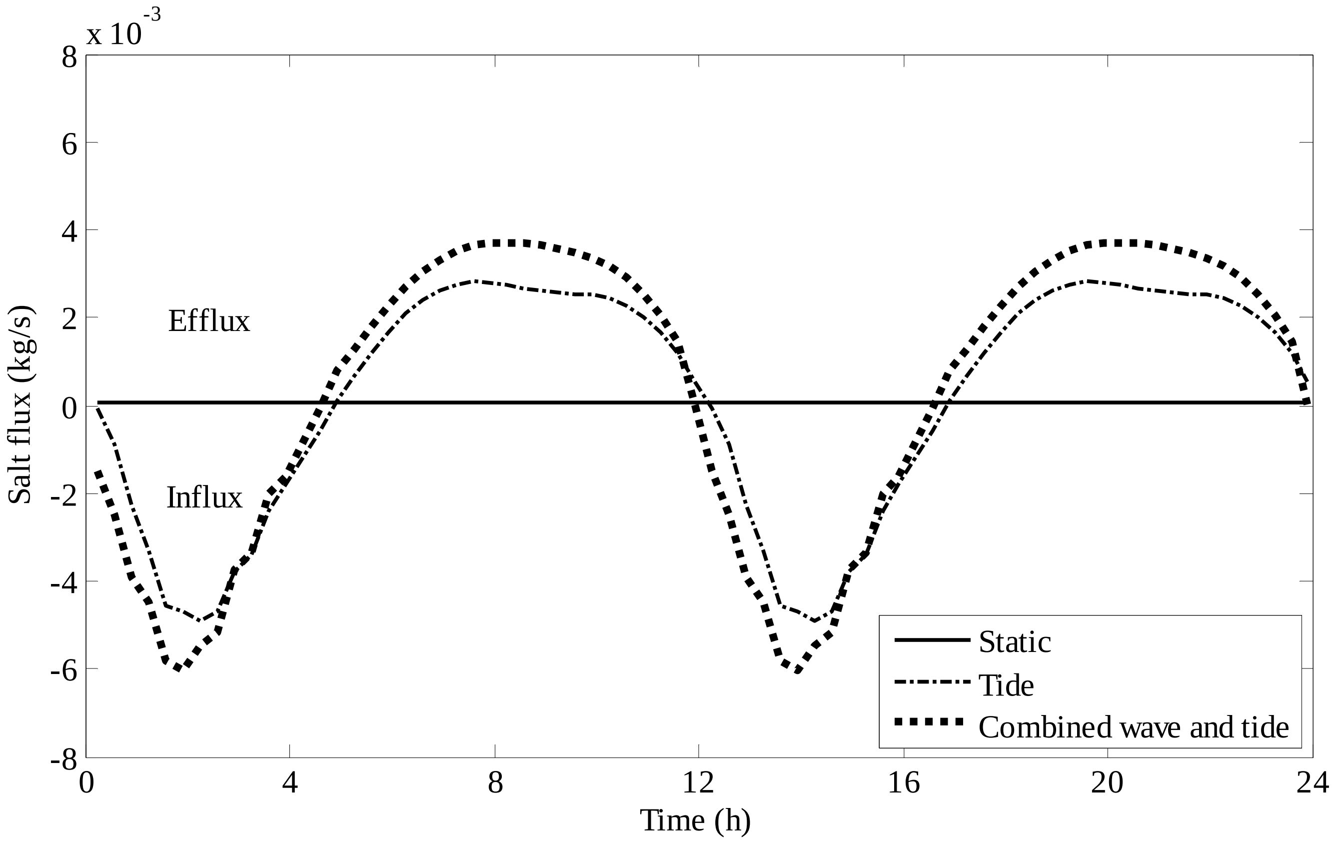
x 10^-3
Salt flux (kg/s)
Efflux
Influx
8
6
4
2
0
-2
-4
-6
-8
0
4
8
12
16
20
24
Time (h)
Static
Tide
Combined wave and tide